PLASTIC UPCYCLING

Low-temperature upcycling of polyolefins into liquid alkanes via tandem cracking-alkylation

Wei Zhang[1]*, Sungmin Kim[2], Lennart Wahl[1], Rachit Khare[1], Lillian Hale[2], Jianzhi Hu[2], Donald M. Camaioni[2], Oliver Y. Gutiérrez[2], Yue Liu[1,3]*, Johannes A. Lercher[1,2]*

Selective upcycling of polyolefin waste has been hampered by the relatively high temperatures that are required to cleave the carbon-carbon (C–C) bonds at reasonably high rates. We present a distinctive approach that uses a highly ionic reaction environment to increase the polymer reactivity and lower the energy of ionic transition states. Combining endothermic cleavage of the polymer C–C bonds with exothermic alkylation reactions of the cracking products enables full conversion of polyethylene and polypropylene to liquid isoalkanes (C_6 to C_{10}) at temperatures below 100°C. Both reactions are catalyzed by a Lewis acidic species that is generated in a chloroaluminate ionic liquid. The alkylate product forms a separate phase and is easily separated from the reactant catalyst mixture. The process can convert unprocessed postconsumer items to high-quality liquid alkanes with high yields.

Plastic is ubiquitous in products that range from packaging and textiles to medical equipment and vehicle components (*1*). More than 360 million tonnes per year (estimated 3 to 4% of the total carbon processed per year) of plastic is produced globally, and most of the disposed plastic accumulates in landfills or is dispersed into water bodies (*2*, *3*). The chemically inert polyolefins, which amount to more than half of all plastics, are challenging to convert below their melting or softening point (*4*). At the present time, recycling technologies are still dominated by mechanical recycling and thermal conversion (incineration and pyrolysis) (*5*, *6*). As a consequence, catalytic upgrading of polyolefin waste into fuels and value-added chemicals has seen substantial research attention, and exciting solutions based on multifunctional catalysts have been emerging (*7*).

Conversion of waste polyolefins is particularly challenging because of the $C(sp^3)$–$C(sp^3)$ bonds, which are more stable than the C-heteroatom bonds of functionalized polymers such as polyesters and polyamides (*8*). Additionally, the endothermic cleavage of the C–C bonds renders processes thermodynamically unfavorable at low temperatures. As a result, converting polyolefins typically requires severe reaction conditions to overcome the kinetic and thermodynamic constraints (*9*). This has been addressed in recent pioneering contributions through the integration of the endothermic C–C cleavage with exothermic reactions—including hydrogenolysis (*10*–*13*), cross-metathesis (*14*, *15*), and aromatization (*16*)—which achieves conversions beyond the equilibria for cracking (fig. S1).

Thermodynamically balancing the exothermic and endothermic kinetically coupled reactions, however, is insufficient to allow for industrially compatible rates below 100°C. The stability of C–C bonds and steric and diffusional barriers that limit the contact of polymer strands with catalytically active sites lead to very slow rates (*17*). As a consequence, most tandem processes require moderate to high reaction temperatures (typically 200° to 250°C) and diverse catalyst functions for relevant conversion rates; these processes lack precise spatiotemporal control over reactive intermediates among catalytic sites (*18*) and complicate product separation and catalyst recovery (*19*). Approaches that would allow selective conversions at substantially lower temperatures would facilitate reactive polymer recycling and open possibilities for decentralized catalytic upgrading.

To achieve this, we turn to coupling cracking of the polymer with alkylation of the formed alkenes by light isoparaffins [isobutane and isopentane (iC_5)]. At present, the refining process is used to produce triple-branched alkanes with a high octane number, which are used in high-octane gasoline (*20*). Conceptually, linking the endothermic

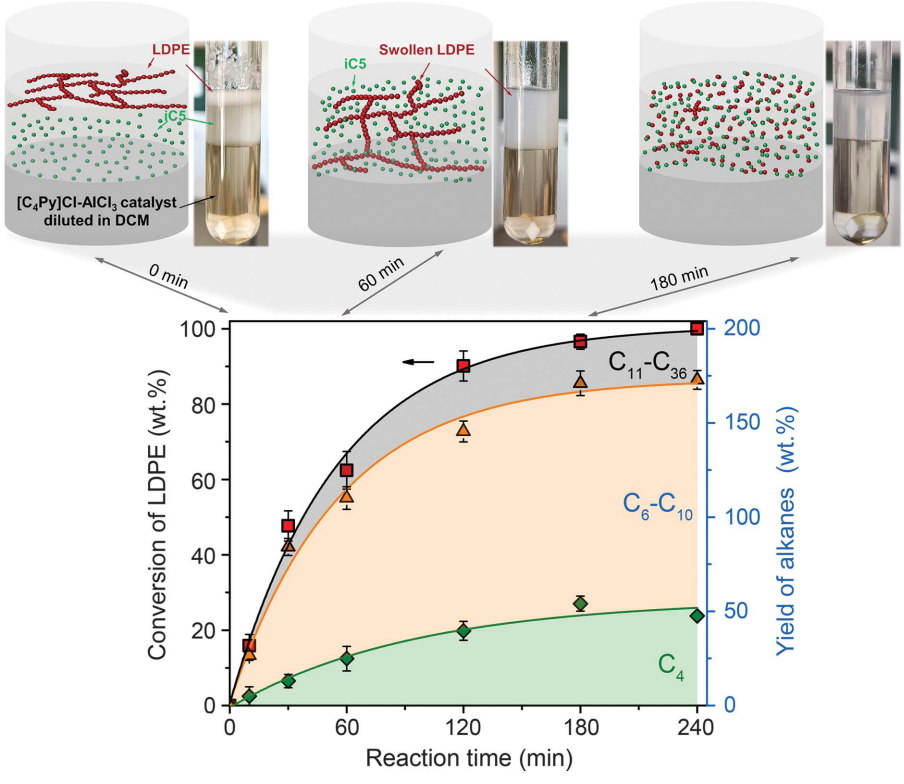

Fig. 1. One-pot catalytic LDPE and iC_5 upcycling into liquid alkanes over Lewis acidic chloroaluminate ionic liquid at 70°C. The time-resolved conversion profile of LDPE and cumulative yield of alkanes (C_4, green diamonds; C_6 to C_{10}, orange triangles; C_{11} to C_{36}, red squares) (bottom). Reaction conditions were as follows: LDPE, 200 mg; iC_5, 800 mg; $[C_4Py]Cl\text{-}AlCl_3$ ($[C_4Py]Cl:AlCl_3$ molar ratio of 1: 2), 3 mmol; TBC as an additive, 0.05 mmol (5 mg); DCM, 3 ml; and temperature, 70°C. The snapshots of the LDPE conversion (top) are at 0, 60, and 180 min from left to right. Curves represent the optimal fit to the data, and all data were repeated at least five times and are shown as mean data points with error bars.

[1]Department of Chemistry and Catalysis Research Center, Technische Universität München, Lichtenbergstr. 4, 85747 Garching, Germany. [2]Institute for Integrated Catalysis, Pacific Northwest National Laboratory, PO Box 999, Richland, WA 99352, USA. [3]Shanghai Key Laboratory of Green Chemistry and Chemical Processes, School of Chemistry and Molecular Engineering, East China Normal University, Shanghai 200062, PR China.
*Corresponding author. Email: w.zhang@tum.de (W.Z.); liuyue@chem.ecnu.edu.cn (Y.L.); johannes.lercher@ch.tum.de (J.A.L.)

cleavage of the polymer C–C bonds to the exothermic alkylation of isoparaffins (i.e., alkylation of the primary alkenes formed from the C–C cleavage by using paraffins whose carbon atoms are retained in the products) couples the two reactions kinetically and, hence, thermodynamically allows full conversion of the polymer below 100°C. All of these reactions are posited to share carbenium ions as intermediates (*21*), which means that they can operate simultaneously within the same medium and with the same catalyst. We showed recently that a highly polar reaction environment strongly increases the standard chemical potential and reactivity of a nonionic reactant (the polymer in this case) and stabilizes the carbenium ion transition states, thereby lowering the overall free-energy barrier of the coupled reactions and notably enhancing reactivity (*22*, *23*).

Combining the concurrent tandem catalysis of cracking-alkylation and polarity-tailored reactant environments, we report here a strategy for the catalytic upgrading of discarded polyolefins and isoparaffins (recycled from the light end of products formed in the process) into gasoline-range alkanes in a single stage. The process enables the upcycling of waste polyethylene with full conversion at 70°C to a narrow distribution of branched liquid alkanes (C_6 to C_{10}) on Lewis acidic chloroaluminate ionic liquid [which is being used as the source of the alkylation catalyst species (*24*)]. Besides its function in generating the active sites, the presence of the high concentration of ions in the ionic liquid is critical for the high conversion rate of the polyolefin at such low temperatures; it not only stabilizes carbenium ions as intermediates, thereby determining the overall reaction rate in the cracking-alkylation reaction, but also allows for easy separation of nonpolar alkane products from the reaction medium.

To visualize the conversion, experiments in glass-tube reactors using commercial low-density polyethylene (LDPE; weight-averaged molecular weight of ~4000, number-averaged molecular weight of ~1700) and iC_5 as substrates (the latter would be replaced by low–molecular weight, branched product alkanes in translation to a semicontinuous process) are shown as examples in Fig. 1. The Lewis acidic chloroaluminate ionic liquid consists of *N*-butylpyridinium chloride and anhydrous $AlCl_3$ in a 1:2 molar ratio and is diluted in the present experiments in dichloromethane (denoted as $[C_4Py]Cl\text{-}AlCl_3$; see the materials and methods for details). The liquid catalyst, together with iC_5, led to complete LDPE conversion at 70°C after 3 hours in the presence of small amounts of *tert*-butyl chloride (TBC) to provide an initial concentration of carbenium ions to start the chain process. The yield of alkane products (C_4 to C_{36}) was twice as high as the amount of LDPE converted, reaching ~200 wt % (this suggests that, on average, an alkene with five C atoms is added relative to initial LDPE, and the stoichiometric mass ratio of LDPE/iC_5 was 1:1; see details in fig. S2); these products were present in the organic phase at the top, which was separated from the inorganic ionic liquid phase at the bottom. The main products were highly branched C_6 to C_{10} liquid alkanes (identified by gas chromatography–mass spectrometry in fig. S3), which accounted for ~126 wt % yield. Other products were gaseous isobutane (iC_4, ~48 wt %) and large alkanes (C_{11} to C_{36}, ~27 wt %). We found only traces of propane and propene (<0.1 wt %) in the headspace (fig. S4). The absence of methane and ethane allows us

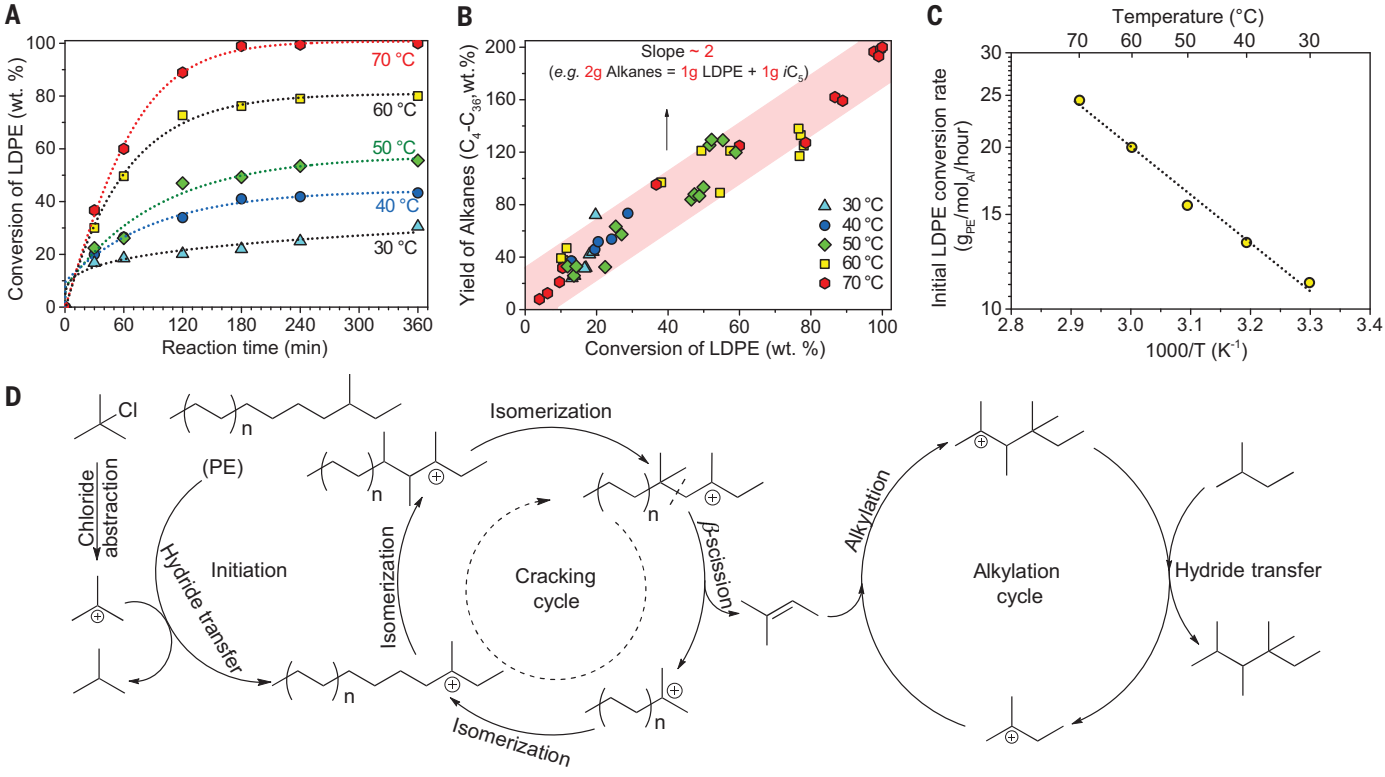

Fig. 2. Low-temperature catalytic performance for LDPE to alkanes and proposed reaction mechanism. (**A**) Time-resolved conversion profile of LDPE in the presence of TBC at different temperatures. Curves represent the optimal fit to the data, and all data were repeated at least five times and are shown as mean data points. (**B**) The corresponding mass yield to alkanes (C_4 to C_{36}) plotted against LDPE conversion. Reaction conditions were as follows: LDPE, 200 mg; iC_5, 800 mg; $[C_4Py]Cl\text{-}AlCl_3$, 3 mmol; TBC, 0.05 mmol; DCM, 3 ml; and temperature, 30° to 70°C. The red-shaded region represents a general linear fit to the data and is used to guide the eye. (**C**) Arrhenius plot for LDPE conversion with initial rates normalized to the aluminum content. (**D**) Proposed reaction mechanism for the tandem cracking-alkylation process of a polyolefin with iC_5. The 2-methyl-butene formed in the cracking cycle is depicted as an example that is based on the ratio of the molecular weight of the carbon products, which suggests that the ratio of converted LDPE and iC_5 is about 1:1 in the reaction, as deduced from Fig. 2B. PE, polyethylene.

to conclude that the reaction occurs overwhelmingly via carbenium ions and does not involve C–C cleavage via carbonium ions (figs. S5 and S6).

The control experiment with LDPE in the absence of iC_5 resulted in only 28 wt % LDPE conversion and produced a red-orange liquid with gaseous products that dominated the product distribution (~39 wt % isobutane and ~26 wt % pentane; see fig. S7). The yield of liquid alkanes in the range of C_6 to C_{10} was only 15 wt % (i.e., lower than the 61 wt % that was observed in the presence of iC_5), whereas the yield of large hydrocarbons (C_{11} to C_{36}) was as high as 20 wt %. In the absence of iC_5, olefinic hydrocarbons likely interact with the chloroaluminate anions, which deactivates the catalyst and yields adamantanes and acid-soluble conjunct polymers (so-called "red oil") (fig. S8) (*25*). In the presence of iC_5, alkanes were preferentially formed and accumulated in the iC_5-containing phase, separated in this way from the polar [ionic liquid with dichloromethane (DCM)] phase. Thus, iC_5 acts as an alkylating agent to form an alkane mixture, which resembles that of an isobutane or *n*-butene alkylation in the refining industry (*24*).

Because $[C_4Py]Cl\text{-}AlCl_3$ ionic liquid contains both Lewis and Brønsted acid sites (fig. S9A), the question arises whether the catalysis follows a reaction pathway that combines carbenium ion formation and sequential reactions catalyzed solely by Lewis acid sites or a reaction pathway that combines the carbonium ions formed by Brønsted acids with sequential reactions of carbenium ions (*26*). Carbenium ions are formed from alkanes at Lewis acid sites via hydride abstraction, whereas strong Brønsted acid sites form carbonium ions on the polymer strands that may crack or eliminate H_2 to form carbenium ions (*27*).

To discern the potential reaction pathways, we added co-reagents, including protic compounds [H_2O and CF_3COOH to generate carbonium ions (*28*)] and TBC [to generate carbenium ions (*29*)]. Adding protic co-reagents did not change the reaction rates or the product distribution compared with the reaction in their absence (see fig. S9B). Although traces of H_2 evolved, other products of protolytic cracking such as methane or ethane were completely absent. Thus, we rule out Brønsted acids and carbonium ions as the pathway to form carbenium ions. By contrast, adding TBC substantially enhanced the initial reaction rate by at least one order of magnitude and led to a nearly full conversion after 180 min, whereas only 20% was converted in its absence (fig. S9, B and C). The nature of the initiator did not markedly influence the rate of reaction (fig. S10, A and B). Control experiments using *n*-hexadecane as a model for LDPE reacting with iC_5 led to an identical enhancement (fig. S10, C and D). Thus, we conclude that most of the carbenium ions are initiated via hydride abstraction from polymer strands by *tert*-butyl carbenium ions formed from TBC, with the reaction propagating via a carbenium ion chain mechanism (*29*). The high reaction rate is determined by the rate of polymer cracking via a carbenium ion chain mechanism, and the faster alkylation of intermediately formed alkenes with an isoalkane (eventually from the light fraction of the products) shifts the equilibrium such that full conversion is possible.

Temperature-dependent experiments (Fig. 2A) showed that the LDPE conversion increased from 20 to 90% after a 2-hour reaction time, when the reaction temperature was raised from 30° to 70°C. The yield of alkanes points to an overall single alkylation step, which leads to a yield of products that is approximately twice the mass of LDPE converted (Fig. 2B). In return, such an average product yield indicates that the average size of the intermediately formed alkene is close to pentene, followed by alkylation with iC_5 to yield decane isomers (fig. S11A). Actually, the main products are branched alkanes, with an average carbon number of ~8.4, which is lower than the theoretical value of 10. The lower carbon production represents higher H/C ratios, which means that the competing cyclization occurs and produces some polycyclic alkanes and acid-soluble oil with decreased H/C ratios. Evidently, the detected cyclohexanes and adamantanes as by-products (fig. S11B) agree well with this trend.

Figure 2C shows the logarithmic dependence of the initial rate of LDPE conversion on the inverse temperature; from this, the apparent activation energy of the overall reaction was 17 ± 2 kJ/mol, which is much lower than the reported apparent activation barriers (163 to 303 kJ/mol) for the depolymerization of polyethylene so far (*19*). We also studied different isoalkanes using iC_4 and iC_6 as alkylating components for LDPE upcycling, which reached nearly 100 wt % of LDPE conversion and yielded branched alkanes (linear alkanes are negligible) under optimal conditions (fig. S12). This result demonstrates the practicability of recycling the lighter alkane product, that is, using iC_4 and iC_5 as the alkylation agents (details of recycling of light isoparaffins are given below).

To account for the tandem reaction proceeding with a constant rate, we posit two (independent) linked catalytic cycles based on carbenium ions, with cracking-derived alkenes serving as the linking intermediates (Fig. 2D). The fundamental differences in the reactivity dictate that in the initial stage of the reaction, hydride transfer from both the isoalkanes and the polyolefin dominates. As the reaction progresses, cracking of the polymer strands becomes predominantly associated with the cooperative action of alkylation. Thus, overall, the observed rates and product distributions are well explained by the two catalytic cycles depicted in Fig. 2D. The reaction is initiated by chloride abstraction from TBC. The formed carbenium ions abstract a hydride, preferentially from tertiary carbon atoms, both at branches in the polymer and in the more abundant iC_5. The carbenium ions formed in the polymer strands tend to undergo skeletal isomerization

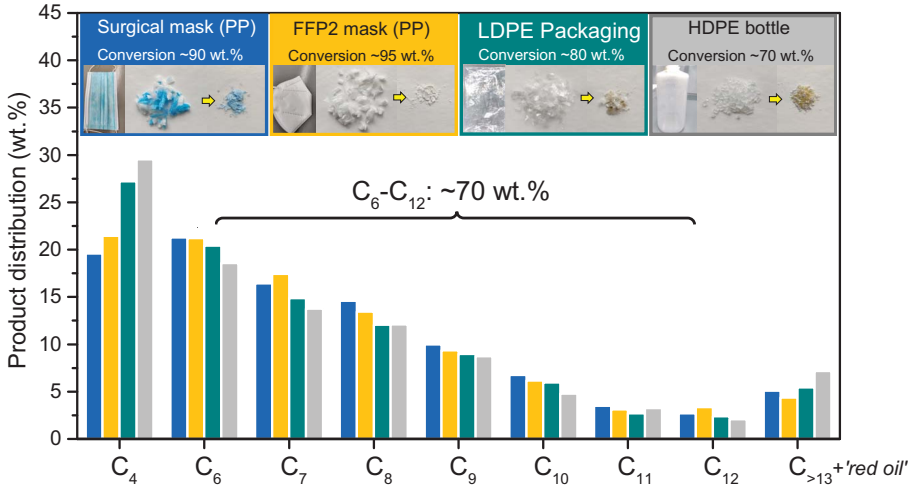

Fig. 3. Selective deconstruction of postconsumer polyolefin waste into liquid alkanes. Product distribution of tandem cracking-alkylation of postconsumer polyolefin waste with iC_5 with $[C_4Py]Cl\text{-}AlCl_3$. No methane, ethane, or propane was detected; all products were branched alkanes. Reaction conditions were as follows: polyolefin waste, 200 mg; iC_5, 800 mg; $[C_4Py]Cl\text{-}AlCl_3$, 3 mmol; TBC, 0.05 mmol; and DCM, 3 ml. Reaction temperatures and times were as follows: disposable surgical mask, 70°C for 6 hours; FFP2 mask, 70°C for 6 hours; food packaging, 70°C for 48 hours; and HDPE bottle, 100°C for 48 hours. PP, polypropylene; FFP, filtering face piece.

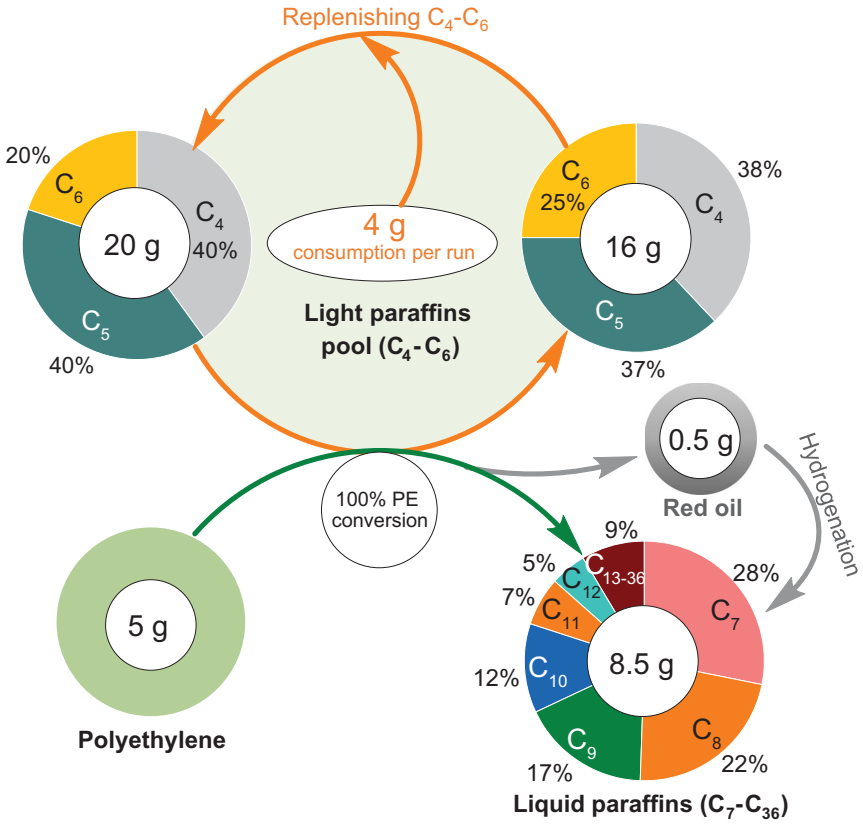

Fig. 4. Full conversion of polyethylene and isoparaffins that are recycled from the light products formed in the process. Cracking-alkylation of LDPE with light paraffin mixture (C_4 to C_6) as recycled light products from polyolefin deconstruction, which gives full LDPE conversion and branched C_{7+} alkanes. Each run only consumed 4 g of light paraffins from the pool, yielding 8.5 g of liquid isoparaffins (C_7 to C_{36}) and a minor amount of red oil as side products (0.5 g) that can easily hydrogenate to saturated hydrocarbons (fig. S20). Reaction conditions were as follows: LDPE, 5 g; initial light paraffin pool, 20 g (C_4, 40 wt %; C_5, 40 wt %; C_6, 20 wt %); [C_4Py]Cl-$AlCl_3$, 30 mmol; TBC, 100 mg; DCM, 75 ml; 2 MPa (N_2); temperature, 70°C; and reaction time, 2 hours.

and cracking via β-scission. Alkenes formed in this process (cracking cycle) react with carbenium ions formed from isoalkanes in the alkylation cycle. The detailed pathways using *n*-hexadecane as a model for LDPE are shown in figs. S13 and S14. The chemistry observed in this latter cycle is identical to that of the alkylation of isobutane with *n*-butene on such ionic liquid-based catalysts (*30*). Unless terminated by hydrogen transfer, these two cycles operate independently from each other, with their relative rates determining the product distribution. The rate of cracking in these coupled processes allows the use of an unusually low concentration of isoalkanes in the overall pool of reactive substrates compared with conventional isobutane and *n*-butene alkylation.

The final question to be addressed is the nature of the active sites that initiate and stabilize the chain propagation and catalysis that was observed. The speciation of [C_4Py]Cl-$AlCl_3$ ionic liquid depends closely on the initial ratio between *N*-butylpyridinium chloride and anhydrous aluminum chloride, in which monomeric $AlCl_4^-$ and dimeric $Al_2Cl_7^-$ dominate at equilibrium (fig. S15). In situ ^{27}Al magic-angle spinning nuclear magnetic resonance spectroscopy (^{27}Al MAS NMR) and Raman spectroscopy showed that increasing the initial fraction of anhydrous aluminum chloride promotes the transformation from $AlCl_4^-$ to $Al_2Cl_7^-$, which in turn results in improved reaction rates (fig. S16). The observed catalytic behavior seems to be determined by the Lewis acidic $Al_2Cl_7^-$ anions (fig. S17), which were generally proposed as the catalytically active sites for catalysis over past decades (*31*). Intriguingly, further kinetic analysis uncovered that the reaction rate was not proportional to the concentration of $Al_2Cl_7^-$ (fig. S18) but rather to the transient aluminum trichloride ($AlCl_3$*) derived from the dissociation of $Al_2Cl_7^-$ (fig. S19). Unlike anhydrous aluminum chloride that features dimeric Al_2Cl_6, $AlCl_3$* species were undetectable and typically ignored because of the extremely small value of the equilibrium dissociation constant (*26*). To substantiate this inference, we plotted, in fig. S19, the turnover frequencies of [C_4Py]Cl-$AlCl_3$ against the concentration of $AlCl_3$*, which showed a linear correlation. Thus, we conclude that increasing the molar ratio of $AlCl_3$ to [C_4Py]Cl increases the concentration of dimeric $Al_2Cl_7^-$ species, which in turn results in an increased concentration of $AlCl_3$* active species.

The strategy described can near-quantitatively convert a wide selection of polymer consumer products with selectivity to C_6 to C_{12} products totaling more than 70 wt %, as exemplified by the results of reactions run using face masks, food packaging, and a high-density polyethylene (HDPE) bottle (Fig. 3). Depolymerization of HDPE bottles is less straightforward because of their compact structure, which lowers the contact surface or site between catalyst and granules, and will require further practical measures to increase dispersion. In practical implementation, the formed light isoalkanes (C_4 to C_6) can be recycled back as alkylating agents, which will ideally enable full conversion (because we hardly produce other light alkanes, including methane, ethane, and propane). To test this, we used the light isoparaffins mixture (C_4 to C_6) as the alkylating component for LDPE upcycling to simulate the recycling experiments, which reached full LDPE conversion and yielded branched alkanes (linear alkanes are negligible) (Fig. 4). Repeated batch experiments showed that the [C_4Py]Cl-$AlCl_3$ catalyst retained its activity and can be used at least five times without regeneration, thereby constantly reaching full LDPE conversion (fig. S20A). Some minor by-products, including red oil complexed with chloroaluminate anions, can be easily converted into saturated hydrocarbons via hydrogenation (fig. S20, B and C), which regenerates the [C_4Py]Cl-$AlCl_3$ ionic liquid. These results demonstrate the practicability of recycling the lighter alkane product as the alkylation agent. Although practical challenges will exist, scaling these results to a quasi-continuous process (conceptualized in fig. S21) is concluded to be highly promising and will integrate recycling of all light hydrocarbons or polymer swelling components.

Acidic chloroaluminate-based ionic liquids as emerging alkylation catalysts have already been industrially used in the paraffin alkylation process at Chevron's Salt Lake City refinery and China National Petroleum Corporation (CNPC), which demonstrates the stability of such catalysts (*32*). We thus envision that this upcycling strategy can be rapidly implemented not only in newly designed plants but also in existing refining technology. The synchronous release of alkenes via polyolefin cracking in the presented cascade cracking-alkylation conceptually allows for better control of product distribution and minimization of the formation of red oil waste (*27*), making polyolefins a

potential feed for refining alkylation. This work opens a transformative scalable approach to convert polyolefins and enables a critical contribution to a circular carbon economy.

REFERENCES AND NOTES

1. R. Geyer, J. R. Jambeck, K. L. Law, *Sci. Adv.* **3**, e1700782 (2017).
2. J. M. Garcia, M. L. Robertson, *Science* **358**, 870–872 (2017).
3. G. W. Coates, Y. D. Y. L. Getzler, *Nat. Rev. Mater.* **5**, 501–516 (2020).
4. S. C. Kosloski-Oh, Z. A. Wood, Y. Manjarrez, J. P. de Los Rios, M. E. Fieser, *Mater. Horiz.* **8**, 1084–1129 (2021).
5. Z. O. G. Schyns, M. P. Shaver, *Macromol. Rapid Commun.* **42**, e2000415 (2021).
6. S. M. Al-Salem, A. Antelava, A. Constantinou, G. Manos, A. Dutta, *J. Environ. Manage.* **197**, 177–198 (2017).
7. A. J. Martín, C. Mondelli, S. D. Jaydev, J. Pérez-Ramírez, *Chem* **7**, 1487–1533 (2021).
8. I. Vollmer *et al*., *Angew. Chem. Int. Ed.* **59**, 15402–15423 (2020).
9. L. O. Mark, M. C. Cendejas, I. Hermans, *ChemSusChem* **13**, 5808–5836 (2020).
10. G. Celik *et al*., *ACS Cent. Sci.* **5**, 1795–1803 (2019).
11. J. E. Rorrer, G. T. Beckham, Y. Román-Leshkov, *JACS Au* **1**, 8–12 (2020).
12. A. Tennakoon *et al*., *Nat. Catal.* **3**, 893–901 (2020).
13. S. Liu, P. A. Kots, B. C. Vance, A. Danielson, D. G. Vlachos, *Sci. Adv.* **7**, eabf8283 (2021).
14. X. Jia, C. Qin, T. Friedberger, Z. Guan, Z. Huang, *Sci. Adv.* **2**, e1501591 (2016).
15. N. Morlanés, S. G. Kavitake, D. C. Rosenfeld, J.-M. Basset, *ACS Catal.* **9**, 1274–1282 (2019).
16. F. Zhang *et al*., *Science* **370**, 437–441 (2020).
17. D. P. Serrano, J. Aguado, J. M. Escola, *ACS Catal.* **2**, 1924–1941 (2012).
18. H. Yan *et al*., *Science* **371**, 1257–1260 (2021).
19. L. D. Ellis *et al*., *Nat. Catal.* **4**, 539–556 (2021).
20. GlobalData, "Refinery alkylation units market installed capacity and capital expenditure (CapEx) forecast by region and countries including details of all active plants, planned and announced projects, 2022-2026," Report code GDGE1353ICR (2021).
21. A. Feller, I. Zuazo, A. Guzman, J. O. Barth, J. A. Lercher, *J. Catal.* **216**, 313–323 (2003).
22. N. Pfriem *et al*., *Science* **372**, 952–957 (2021).
23. L. Milaković, P. H. Hintermeier, Y. Liu, E. Baráth, J. A. Lercher, *Angew. Chem. Int. Ed.* **60**, 24806–24810 (2021).
24. H. K. C. Timken, S. Elomari, S. Trumbull, R. Cleverdon, "Integrated alkylation process using ionic liquid catalysts," US Patent 7,432,408 (2008).
25. C. J. Adams, M. J. Earle, K. R. Seddon, *Green Chem.* **2**, 21–24 (2000).
26. J. Estager, J. D. Holbrey, M. Swadźba-Kwaśny, *Chem. Soc. Rev.* **43**, 847–886 (2014).
27. A. Feller, J. A. Lercher, in *Advances in Catalysis*, H. Knüpffer, Ed. (Academic Press, 2004), vol. 48, pp. 229–295.
28. A. S. Amarasekara, *Chem. Rev.* **116**, 6133–6183 (2016).
29. S. Aschauer, L. Schilder, W. Korth, S. Fritschi, A. Jess, *Catal. Lett.* **141**, 1405–1419 (2011).
30. Y. Chauvin, A. Hirschauer, H. Olivier, *J. Mol. Catal.* **92**, 155–165 (1994).
31. R. Kore *et al*., *ACS Catal.* **7**, 7014–7028 (2017).
32. H. K. Timken, H. Luo, B.-K. Chang, E. Carter, M. Cole, in *Commercial Applications of Ionic Liquids*, M. B. Shiflett, Ed. (Springer, 2020), pp. 33–47.

ACKNOWLEDGMENTS

We thank A. Wellmann, H. Xu, B. Yang, and J. Mai from the Technische Universität München for their assistance in experiment setup and data collection. We thank W. Hu from Pacific Northwest National Laboratory for support with in situ NMR measurements. We also thank G. L. Haller (Yale University) for his careful reading of the manuscript and helpful suggestions. **Funding:** This work was supported by the US Department of Energy, Office of Science, Office of Basic Energy Sciences, Division of Chemical Sciences, Geosciences and Biosciences (Toward a polyolefin-based refinery: Understanding and controlling the critical reaction steps, FWP 78459) (J.A.L., O.Y.G., J.H., S.K., D.M.C., and L.H.). **Author contributions:** W.Z., Y.L., and J.A.L. conceived the research; W.Z. carried out the reactions and performed the characterizations for selected materials. J.H., S.K., and L.W. provided data on the in situ NMR measurements. R.K., L.H., D.M.C., and O.Y.G. contributed to the discussion and helped to revise the manuscript. All authors contributed to the writing of the manuscript. **Competing interests:** The authors declare that they have no competing interests. **Data and materials availability:** All data are available in the main text or the supplementary materials.

SUPPLEMENTARY MATERIALS

science.org/doi/10.1126/science.ade7485
Materials and Methods
Figs. S1 to S21
References (*33*–*49*)

Submitted 5 September 2022; accepted 30 January 2023
10.1126/science.ade7485

Science
AAAS

Supplementary Materials for

Low-temperature upcycling of polyolefins into liquid alkanes via tandem cracking-alkylation

Wei Zhang *et al*.

Corresponding authors: Wei Zhang, w.zhang@tum.de; Yue Liu, liuyue@chem.ecnu.edu.cn; Johannes A. Lercher, johannes.lercher@ch.tum.de

Science **379**, 807 (2023)
DOI: 10.1126/science.ade7485

The PDF file includes:

Materials and Methods

All chemicals were purchased from Sigma-Aldrich and were used without further purification: low-density polyethylene (LDPE, average $M_w \sim 4000$, average $M_n \sim 1700$), *n*-hexadecane (*n*-$C_{16}H_{34}$, ≥ 99%), 2-methylbutane (isopentane, ≥ 99%), N-butylpyridinium chloride ([C_4Py]Cl, ≥ 98%), anhydrous aluminum (III) chloride (99.99 %), *trans*-decahydronaphthalene (*trans*-Decalin, 99%), dichloromethane (DCM, ≥ 99.5%), chloroform ($CHCl_3$, ≥ 99%), *tert*-butylchloride (TBC, 99%), *tert*-pentylchloride (98%), 1-chloro-2-methylbutane (96%), 1-chloro-2-methylpropane (98%), 2-Methyl-2-butene (99%), *tert*-butylbromide (98%), *tert*-butyliodide (95%).

Procedure for Lewis acidic N-butyl pyridinium chloride-aluminum chloride ionic liquid ([C_4Py]Cl-$AlCl_3$) preparation

The acidic [C_4Py]Cl-$AlCl_3$ is a room-temperature molten salt prepared by mixing N-butyl pyridinium chloride([C_4Py]Cl) and anhydrous aluminum chloride at a 1:2 molar ratio under an inert atmosphere. In a typical synthesis of [C_4Py]Cl-$AlCl_3$ ionic liquid, anhydrous aluminum chloride (6 mmol) was slowly added to [C_4Py]Cl (3 mmol) in a Schlenk flask at room temperature inside a glove box. Note that the reaction is exothermic and needs to cool down and continue stirring to maintain a low temperature, yielding a light-grey liquid.

Procedure for the tandem cracking-alkylation reaction of polyolefin with isopentane

In a typical reaction, low-density polyethylene (LDPE, 200 mg), isopentane (iC_5, 800 mg) and *tert*-butylchloride (TBC, 5 mg) were added into a 30 mL DURAN® borosilicate glass tube (equipped with an open-top screw cap with silicone liner) containing 3 mmol of [C_4Py]Cl-$AlCl_3$ diluted in dichloromethane (DCM, 3 mL). Then, the tube reactor was heated to 70 °C for 3 hours under magnetic stirring (1200 rpm). After the reaction, the tube reactor was first cooled down to room temperature, resulting in a biphasic system with the hydrocarbon products, unreacted swollen polymer, and excess isopentane phase on top and the inorganic ionic liquid and DCM phase on the bottom.

Procedure for product analyses

The reaction products are distributed in the headspace, upper organic phase, as well as the lower inorganic ionic liquid phase. First, the headspace of the reactor was analyzed to quantify the gaseous hydrocarbons using a gas chromatograph (GC, HP 5890) equipped with a Supel-Q™ PLOT fused silica capillary column (30 m × 0.53 mm × 2.0 μm) and a mass spectrometer, which calibrated by standard hydrocarbons (methane, ethane, ethene, propane, propene, and n-pentane. Then, the tube reactor was cooled to -20 °C for 30 min and an additional 2 mL of isopentane was added as an extracting agent that resulted in thorough phase separation. Hydrocarbon products (≥C_4) are mainly in the top organic phase together with minor organic residues in the inorganic ionic liquid on the bottom (The inorganic ionic liquid phase was first transferred to a glass vial and quenched by NaOH aqueous solution at low temperature, and organic residues were extracted by chloroform). All of the products were mixed with 15 mg of trans-decalin as an external standard and analyzed by gas chromatography-mass spectrometry (Agilent, GC-MS 2010) equipped with an HP-5 Agilent column (30 m × 0.32 mm × 0.25 μm). The response factor for alkanes of each carbon number

and the corresponding retention time were calibrated using n-alkane standard (C_7- C_{40}, Supeco-49452-U). A representative GC trace of liquid phase is shown in Fig. S4. The unreacted LDPE suspended solids were separated from the top phase by a simple filtration to quantify the conversion:

$$\text{Conversion} = \left(1 - \frac{\text{mass of residual LDPE}}{\text{initial mass of LDPE}}\right) \times 100\%$$

Quantification of the hydrocarbon C_i (with *i*-th carbons) was determined from the GC-FID signal using external standard reference:

$$\text{Yield}\,(C_i, \%) = \left(\frac{\text{mass of } C_i}{\text{initial mass of LDPE)}}\right) \times 100\%$$

$$= \left(\frac{\sum \text{Area}(C_i)}{\text{Area(external standard)}} \times \frac{\text{mass of external standard}}{\text{initial mass of LDPE}}\right) \times 100\%$$

where $\sum \text{Area}(C_i)$ is the sum of GC areas of C_i, in which all peaks between n-C_{i-1} and n-C_i were assumed as branched C_i alkanes unless GC-MS suggested otherwise. Area (external standard) is the GC area of the external standard. Note that all products and external standard are saturated hydrocarbons; the relative response factors for each species were assumed to be 1.0.

The selectivity of the hydrocarbon C_i (with *i*-th carbons) was calculated as:

$$\text{Selectivity}\,(C_i, \%) = \left(\frac{\text{Yield}\,(C_i)}{\sum \text{Yield}\,C_{\text{total}}}\right) \times 100\%$$

Where $\sum \text{Yield}\,C_{\text{total}}$ is the sum of hydrocarbons in the headspace, the organic phase, and the ionic liquid phase. The mass balances in all experiments were at least 95%. All data were repeated at least five times and are shown as data points either with error bars or as the average of all repetitions in the figures.

Procedure for the recycling tests of $[C_4Py]Cl$-$AlCl_3$ catalyst in the tandem catalytic cracking-alkylation

In a typical recycling experiment, the reactor was cooled down to -20 °C for 30 min after the LDPE/isopentane mixture was reacted, resulting in phase separation. The upper (hydrocarbons + unreacted swollen LDPE) layer was drawn off under low temperatures. Next, fresh LDPE/isopentane together with TBC additive were replenished into the reactor to achieve the predetermined concentrations. Then the reaction system was heated to 70 °C and stirred for a predetermined time until the LDPE was fully consumed. Note that chloroaluminate ionic liquid easily hydrolyzes to release HCl gas and lead to catalyst deactivation, therefore, all operations were handled in an inert atmosphere and at low temperatures.

In situ ^{27}Al MAS NMR spectroscopy measurements

In situ ^{27}Al magic-angle spinning (MAS) nuclear magnetic resonance (NMR) spectroscopy measurements were conducted on a Varian-Agilent Inova wide-bore 300 MHz NMR spectrometer using a commercial 7.5 mm Vespel pencil type MAS probe, operating at ^{27}Al Larmor frequencies of 78.204 MHz. A sample spinning rate of ~4 kHz was used to produce

a high-resolution MAS NMR spectrum. A special *in situ* MAS NMR rotor capable of perfectly sealing a mixture at elevated temperature and pressure was used (*33*). The volume of the sample cell space was ~300 μL. A single pulse sequence was used for acquiring a ^{27}Al signal, consisting of a pulse with a width of 5 μs (equivalent to a pulse angle of 50 °), an acquisition time of 50 ms, and a recycle delay of 0.5 s. All spectra were externally referenced to 1 M $Al(NO_3)_3$ (0 ppm) aqueous solution (*34*).

Raman Spectroscopy measurements

Raman spectra were measured on a Renishaw inVia Reflex Raman System. The spectrometer was combined with an optical light microscope Leica DM2700M from Leica Microsystems Vertrieb GmbH for focusing the Raman laser. The laser was a 532 nm laser RL532C. The laser intensity on the sample was 200 mW. The spectra were collected for a total of 50 s acquisition time with the corrected background.

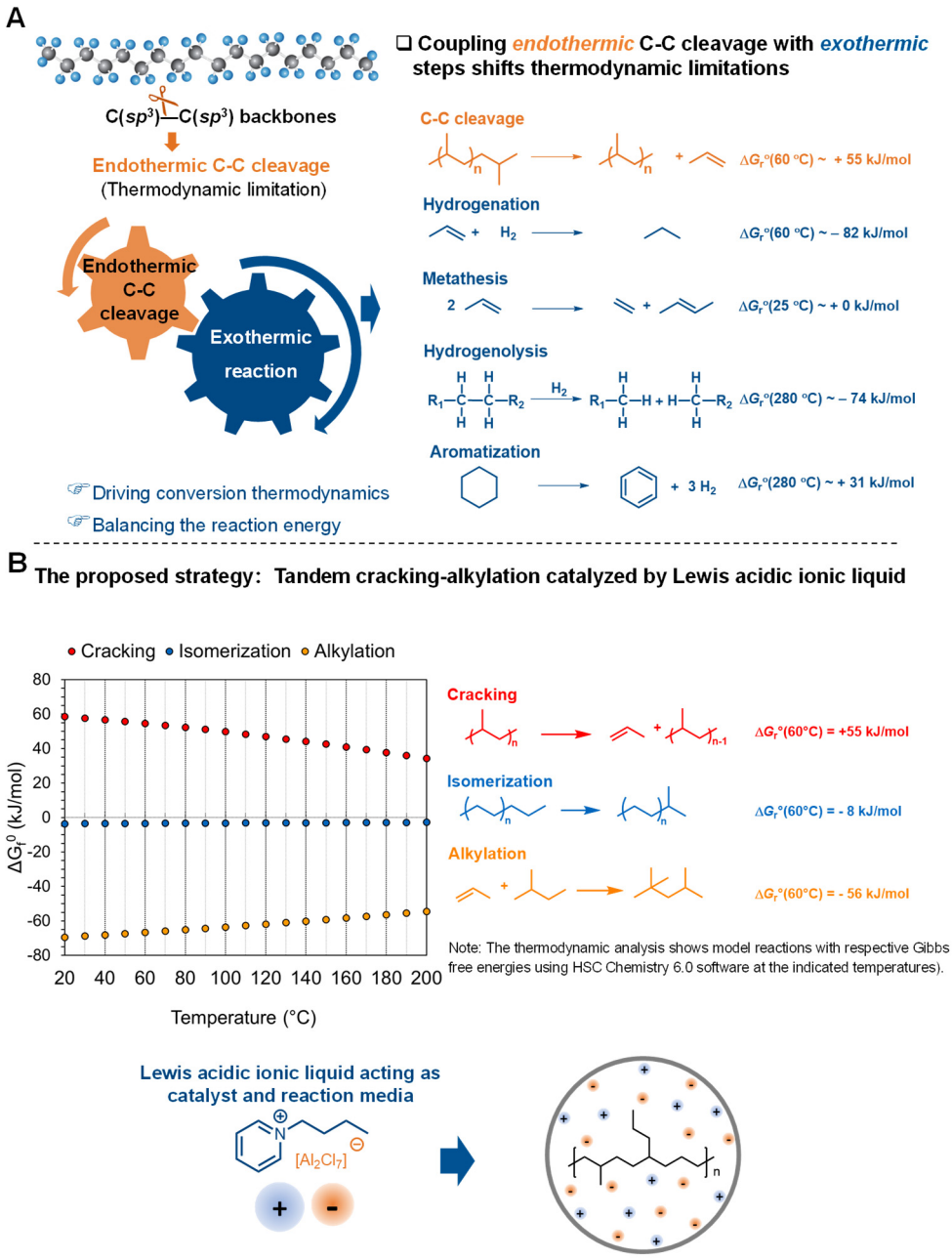

Fig. S1. Current and proposed processes for catalytic upcycling of polyolefin. (**A**) A summary of current coupling of endothermic C-C cleavage with exothermic reactions including hydrogenation/hydrogenolysis (*10-13*), cross-metathesis (*14, 15*), and hydrogenolysis /aromatization (*16*). Note: The thermodynamic values are based on the corresponding reports. (**B**) The proposed tandem cracking-alkylation strategy for catalytic upcycling of polyolefin catalyzed by Lewis acidic ionic liquid, and thermodynamic calculation of model reactions for cracking, alkylation and isomerization with the respective Gibbs free energy of reaction at varying temperatures.

Supplementary Note. The upcycling of polyolefins to lighter hydrocarbons includes inevitable C-C bond cleavage and the formation of alkenes. This cleavage of polymeric C-C bonds is endothermic and, therefore, is thermodynamically limited at low temperatures [ΔG_r^o

(60 °C) ≈ 55 kJ/mol]. To allow for a higher conversion at low temperatures, the endothermic C-C cleavage has to be kinetically coupled to exothermic reactions.

Fig. S1A summarized the recent pioneering works from a thermodynamic perspective, demonstrating the unfavorable thermodynamics of C-C cleavage at low temperatures can be offset by exothermic reactions including hydrogenation, hydrogenolysis, metathesis, and hydrogenolysis-aromatization. Thermodynamic coupling, however, is insufficient on its own to realize high rates of individual reaction steps to convert the polymer at lower than hitherto practiced temperatures. Kinetic control should be achieved for efficient cooperative catalysis. Here we bring this coupling to a new level by combining it with exothermic alkylation catalyzed by ionic liquids, enabling unprecedented low-temperature upcycling of polyolefins. The alkylation of an olefin with an alkane is thermodynamically favored at mild conditions [ΔG_r^o (60 °C) ≈ -56 kJ/mol]. As both reactions share a carbenium ion intermediate, coupling the C-C cleavage with the C-C bond formation and the hydrogen addition via alkylation is conceptually straightforward. Additionally, the slightly exergonic isomerization [ΔG_r^o (70 °C) ≈ -8 kJ/mol] would further assist to yield highly branched hydrocarbons.

Importantly, the reaction media of ionic liquid (e.g., *N*-butylpyridinium chloride/chloro-aluminate ionic liquid) is a medium with high ionic strength and, hence, critical for achieving a high conversion rate of the polyolefins at low temperatures. The high ionic strength of the ionic liquid leads to a positive excess chemical potential of the polyolefin, *i.e.*, it increases its reactivity. The ionic liquid stabilizes, in contrast, the carbenium ions that are involved in all transition states of the two catalytic cycles. Such drastically different stabilization and destabilization of the charged transition states (*e.g.*, the polyolefinic carbenium ions) and the neutral ground states (*e.g.*, the polyolefin ground state), respectively, leads to a drastic lowering of the standard free energy barriers and a corresponding increase in the reaction rates. This effect has also been reported recently, in alcohol dehydration in a concentrated electrolyte solution and in acidic zeolites (*22*).

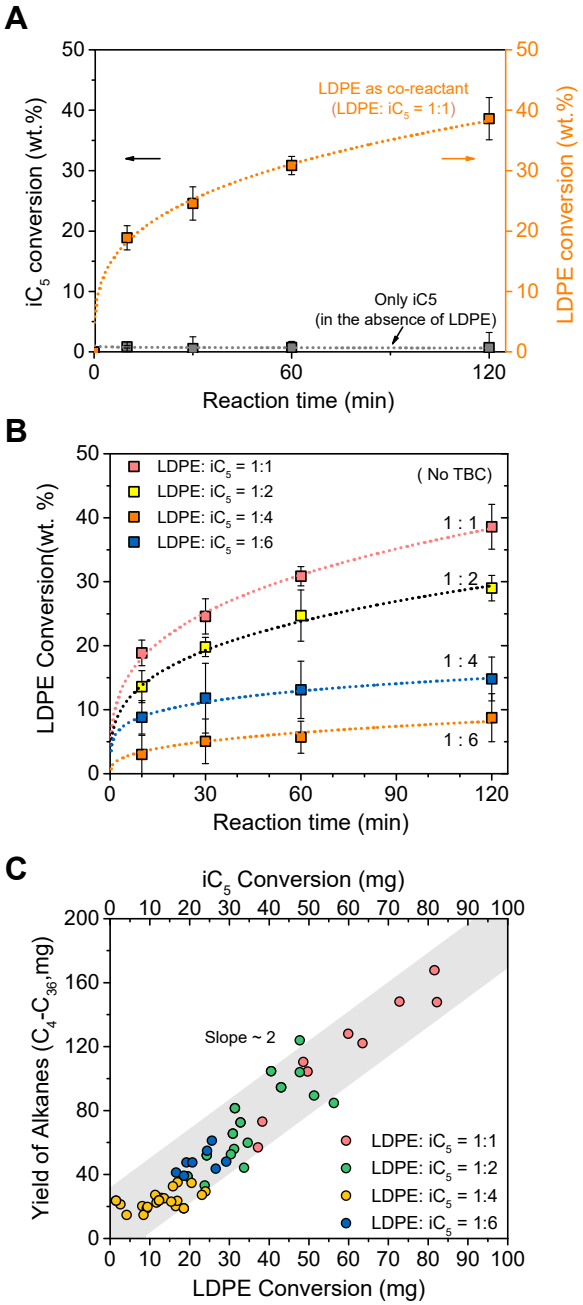

Fig. S2. (**A**)Time-resolved conversion profile of isopentane (iC_5) without/with LDPE as co-reactant. Reaction conditions: (A) iC_5 200 mg (or LDPE 200 mg), [C_4Py]Cl-$AlCl_3$ 3 mmol, DCM 3 mL, 70 °C; (**B**)Time-resolved conversion profile of LDPE with the different mass ratio of LDPE/iC_5 and (**C**) the corresponding mass yield to alkanes (C_4-C_{36}) plotted against LDPE conversion. Reaction conditions: LDPE 200 mg, iC_5/LDPE=1-6, [C_4Py]Cl-$AlCl_3$ 3 mmol, no TBC, DCM 3 mL, 70 °C.

Supplementary Note. The control experiments (Fig. S2A) using only iC_5 (in the absence of LDPE) showed the equilibrium-limited iC_5 transformation (only <1 wt. % conversion), while adding LDPE lead to a dramatic increase in iC_5 conversion reaching 40 wt. % after 120 min. Additionally, we found that LDPE cracking and then alkylate with iC_5 with a stoichiometric mass ratio of 1 to 1. This corroborated the kinetic coupling of cracking-alkylation.

Fig. S2B shows the time-resolved conversion curves of LDPE varying the LDPE/*i*C_5 ratio from 1/1 to 1/6 (without TBC as an additive). The conversion of LDPE tended to increase with a decrease in LDPE/*i*C_5 ratio, and the reaction rate increased as follows: 1/1 > 1/2 > 1/4> 1/6. Too much *i*C_5 dilute the concentration of carbenium ions which reduced the reaction rate. The corresponding mass yield of alkanes displayed a strong linear correlation with both LDPE and *i*C_5 conversions with a slope of ~2 (Fig. S2C). These control experiments further confirm the tandem catalysis between LDPE cracking and iC_5 alkylation with a stoichiometric mass ratio of 1 to 1. Despite the low conversion rate, the high loading of iC_5 does show one important advantage that can suppress the side reaction. Therefore, we decided to focus on the reaction with the fixed LDPE/iC_5 of 1:4 unless suggested otherwise. Overall, the alkylation agent, i.e. exemplified by isopentane here, plays a key role in this reaction: (i) alkylates the primary olefin fragments during polymer cracking, suppressing the complexation with catalyst and reducing the formation of side products (red oil and adamantanes); (ii) they (together with ionic liquid and DCM) lead to polyolefin swelling, increasing the contact between polymer strains and catalyst; and (iii) they act as extracting agent, separating ionic liquids from the alkane products.

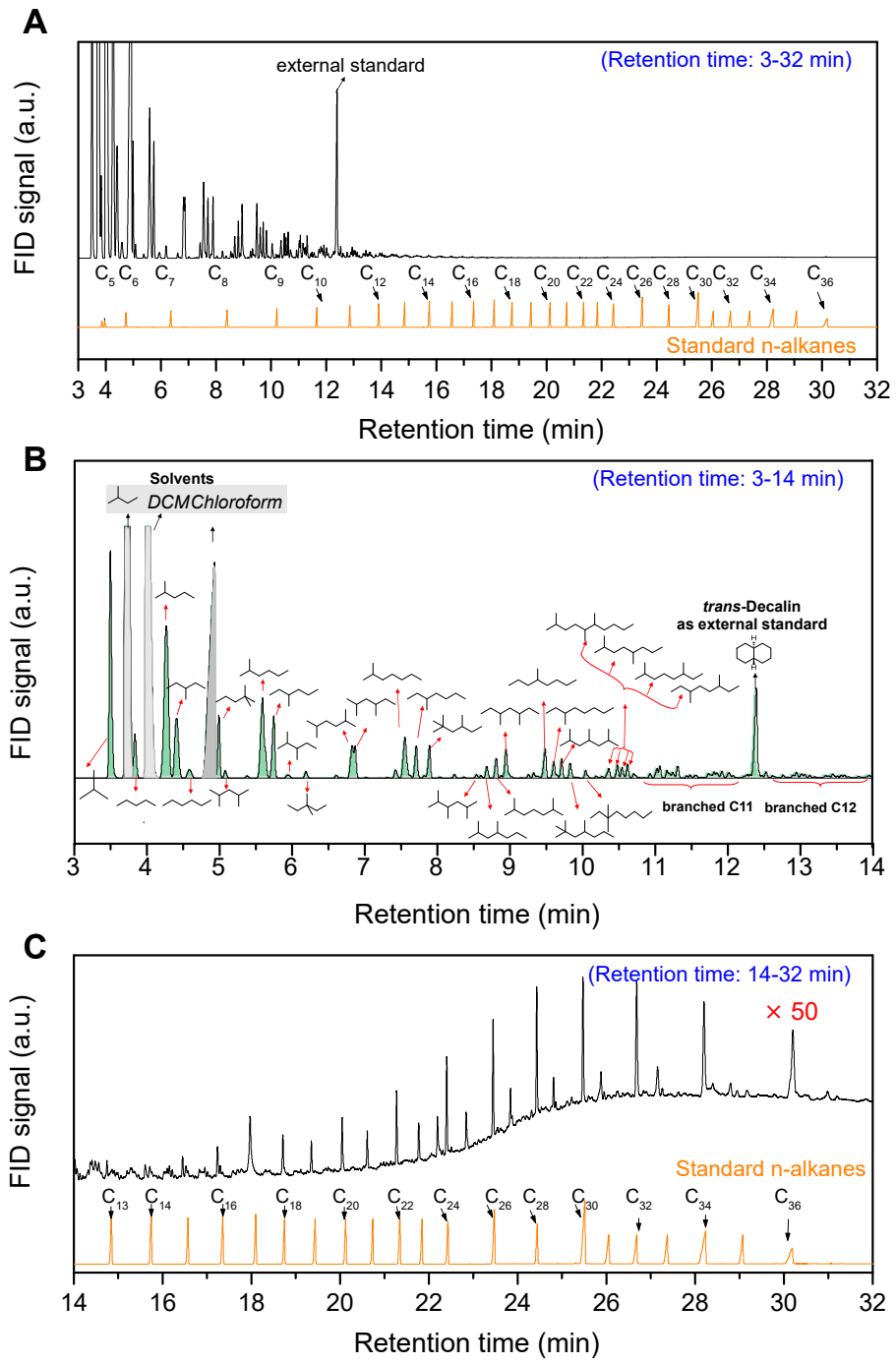

Fig. S3. GC and GC-MS analysis of hydrocarbon products (≥C_4) from the tandem catalytic LDPE/*i*C_5 upcycling (dissolved in *i*C_5, DCM, and chloroform), using n-alkanes as the reference standard. (**A**)The main products are mainly centered on the range of C_4-C_{10} and negligible heavy alkanes (C_{12}-C_{36}). (**B**) GC signals at the retention time from 3–14 min, identified by GC-MS, showing that the liquid alkanes as the main products are highly branched in the range of C_6-C_{10}. (**C**) GC signals (×50) at the retention time from 14–32 min, showing several minor heavy alkane fragments (C_{13}-C_{36}).

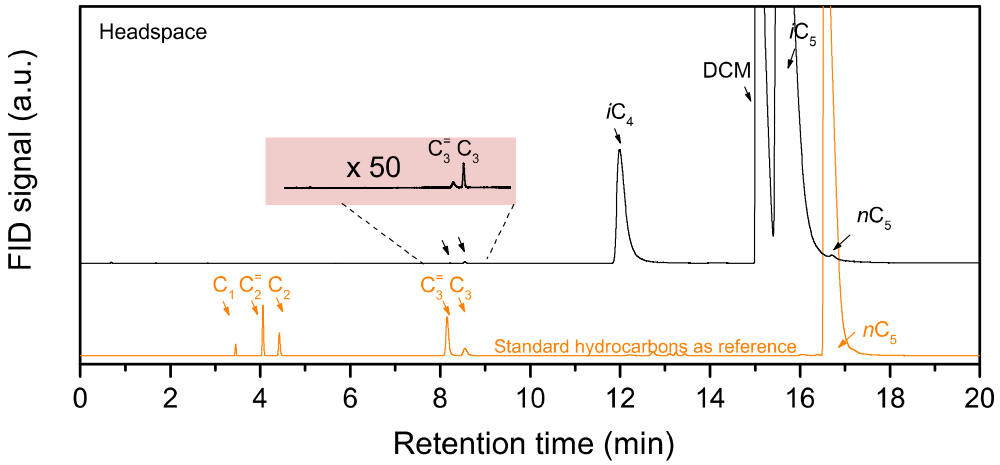

Fig. S4. GC analysis of the headspace from the tandem catalytic LDPE/iC_5 upcycling, which is calibrated by standard hydrocarbons (methane, ethane, ethene, propane, propene and n-pentane).

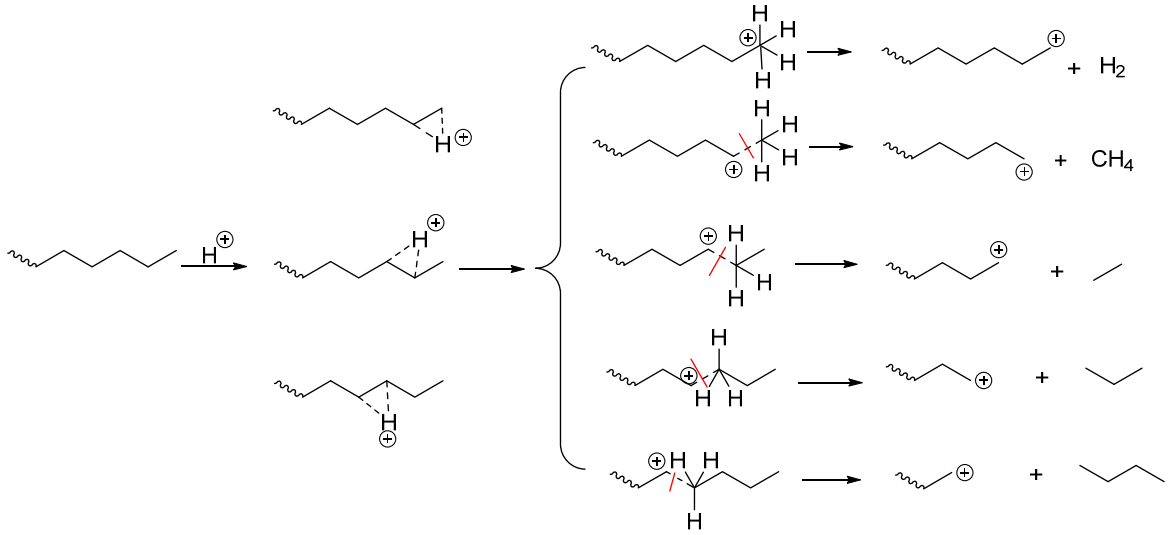

Fig. S5. Illustration of C-C cleavage via penta-coordinated carbonium ion intermediate (*35*), further forming carbenium ions and smaller products including hydrogen, methane and ethane and propane and n-butane. The dotted line represents the location of the bond scission.
Supplementary Note. We concluded that the tandem cracking-alkylation of polyolefin does not involve C-C cleavage via carbonium ions, as methane and ethane were completely absent (evidenced by the GC analysis in Fig. S4).

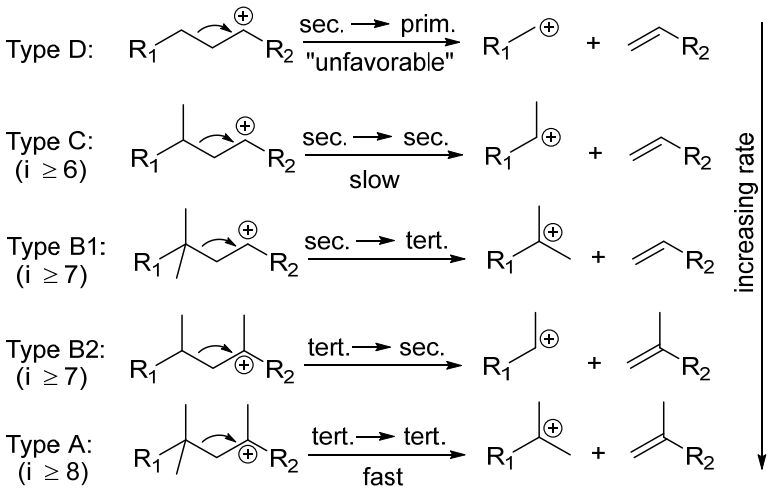

Fig.S6. Classification of *β*-scission reactions of carbenium ions (*36*).

Supplementary Note. The mechanism of the C-C bond cleavage of polyolefin occurred chiefly via the type A *β*-scission mechanism (*36*). In principle, there are mainly five types of *β*-scissions including A, B1, B2, C, and D. Type A starts and ends up in a tertiary carbenium ion of multi-branched isomers with at least eight carbon atoms, producing iC_4 and branched C_{i-4}. Type B requires a minimum of seven carbon atoms and two branches, in which type B1 transforms a secondary carbenium into a tertiary one or vice versa in type B2; The type B *β*-scission can explain the formation of C_3 and C_{i-3} fragments. Only type C occurs in mono-branched isomers with at least six carbon atoms producing two linear paraffins. Type D difficulty occurs due to the high formation energy of primary carbocation. The relative scission rate of carbenium increased with its branching degree, according to the sequence A > B1 = B2 > C ≫ D.

In our case, the carbenium ions are preferentially formed at the branching points of polymer chains. As a result, type A *β*-scission is the predominating cracking mechanism in the multibranched *tert*-carbenium ions, which is in accordance with the feature of our product distribution with the exclusively branched alkanes (propene, propane and other linear alkanes are negligible, see Figs. S3 and S4). It should be noted that in the industrially practiced alkylation (2-butene and iso-butane reacting) alkenes are hardly observed in the product stream (*27*). Actually, alkenes formed in the cracking cycle, followed by a rapid alkylation of alkene/isoparaffin significantly shift the equilibrium via exothermic alkylation of alkene fragments. This explains why only traces of propene are in the headspace.

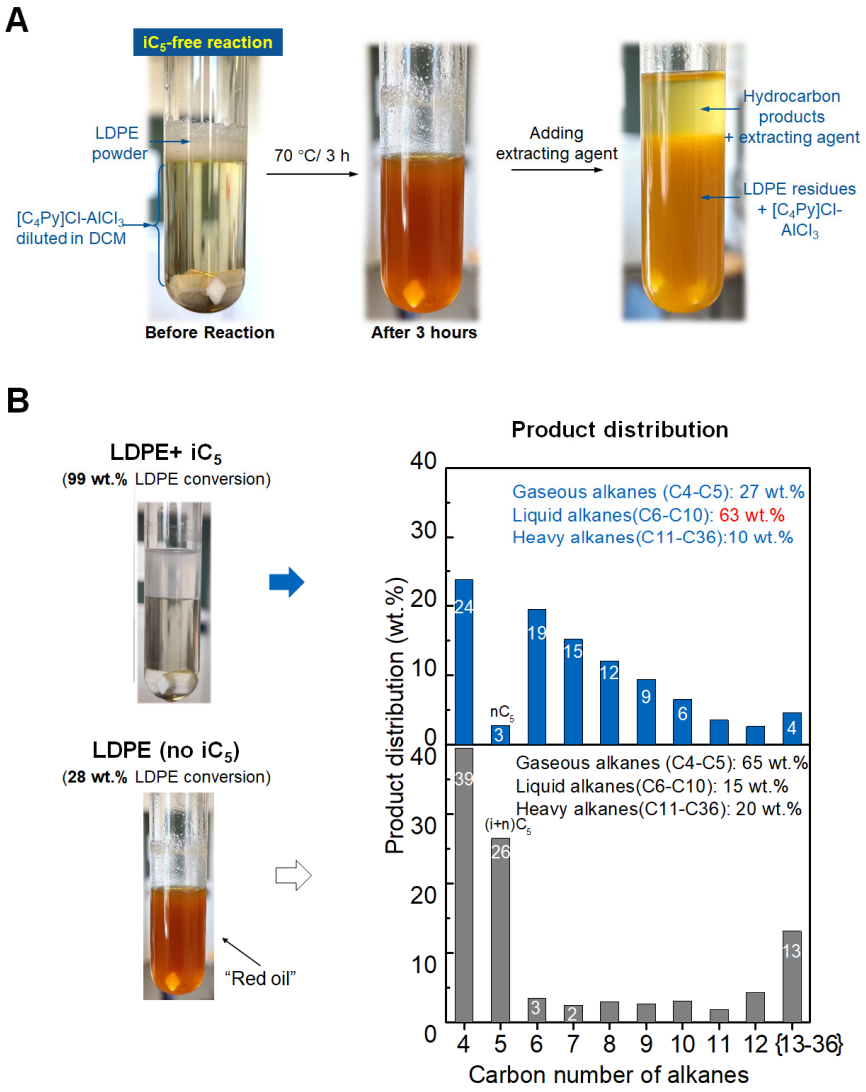

Fig. S7. The *i*C$_5$-free upcycling of LDPE over [C$_4$Py]Cl-AlCl$_3$. (A) The snapshots of the *i*C$_5$-free reaction system after 3 hours and after extraction by cyclohexane. **(B)** Comparison of *i*C$_5$-involved and *i*C$_5$-free upcycling of LDPE over [C$_4$Py]Cl-AlCl$_3$ catalyst, and their corresponding alkane product distribution. Reaction conditions: LDPE 200 mg, isopentane (*i*C$_5$) 800 mg, [C$_4$Py]Cl-AlCl$_3$ 3 mmol, TBC 0.05 mmol (5mg), DCM 3 ml, 70 °C, 3 h.

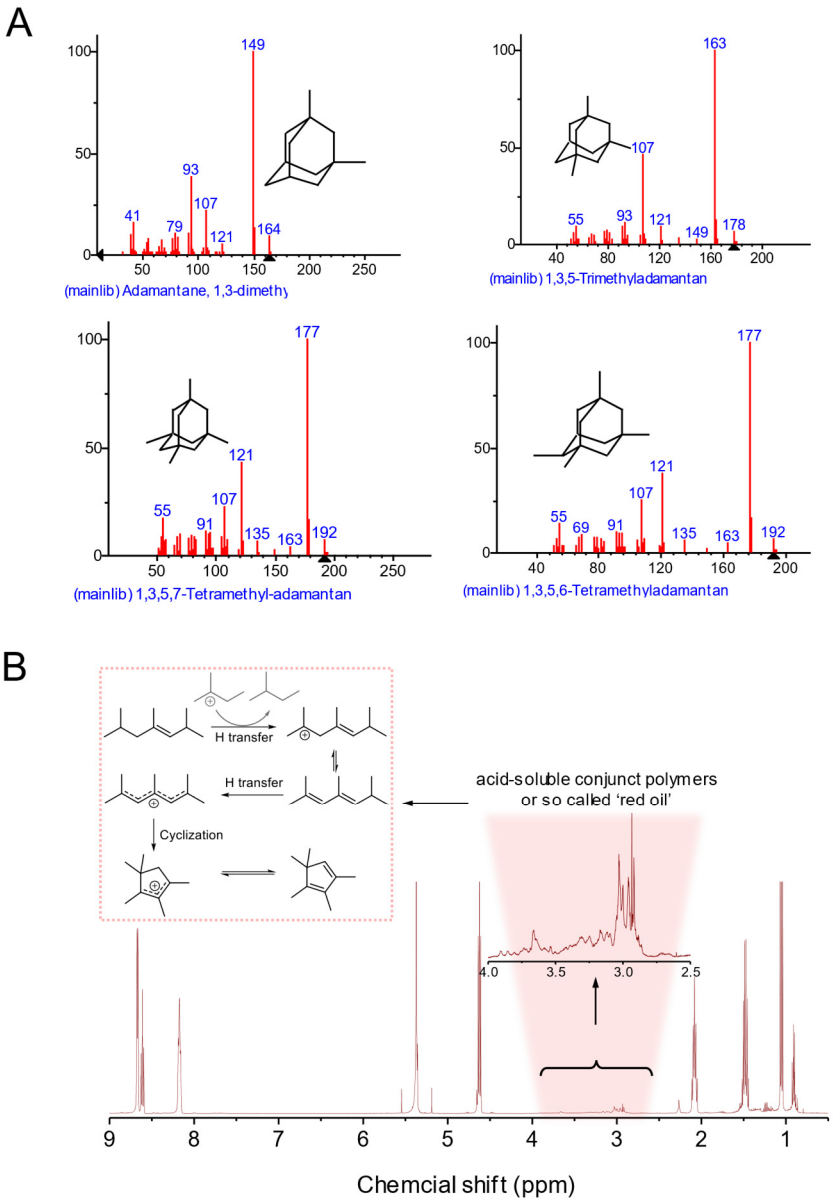

Fig. S8. Side products from *i*C$_5$-free upcycling of LDPE. (**A**)The GC-MS signals and (**B**) ^{1}H NMR spectra of *i*C$_5$-free upcycling of LDPE at 70 °C, 3 h, showing the formation of adamantanes and acid-soluble conjunct polymers (so-called '*red oil*') (*21, 27*).

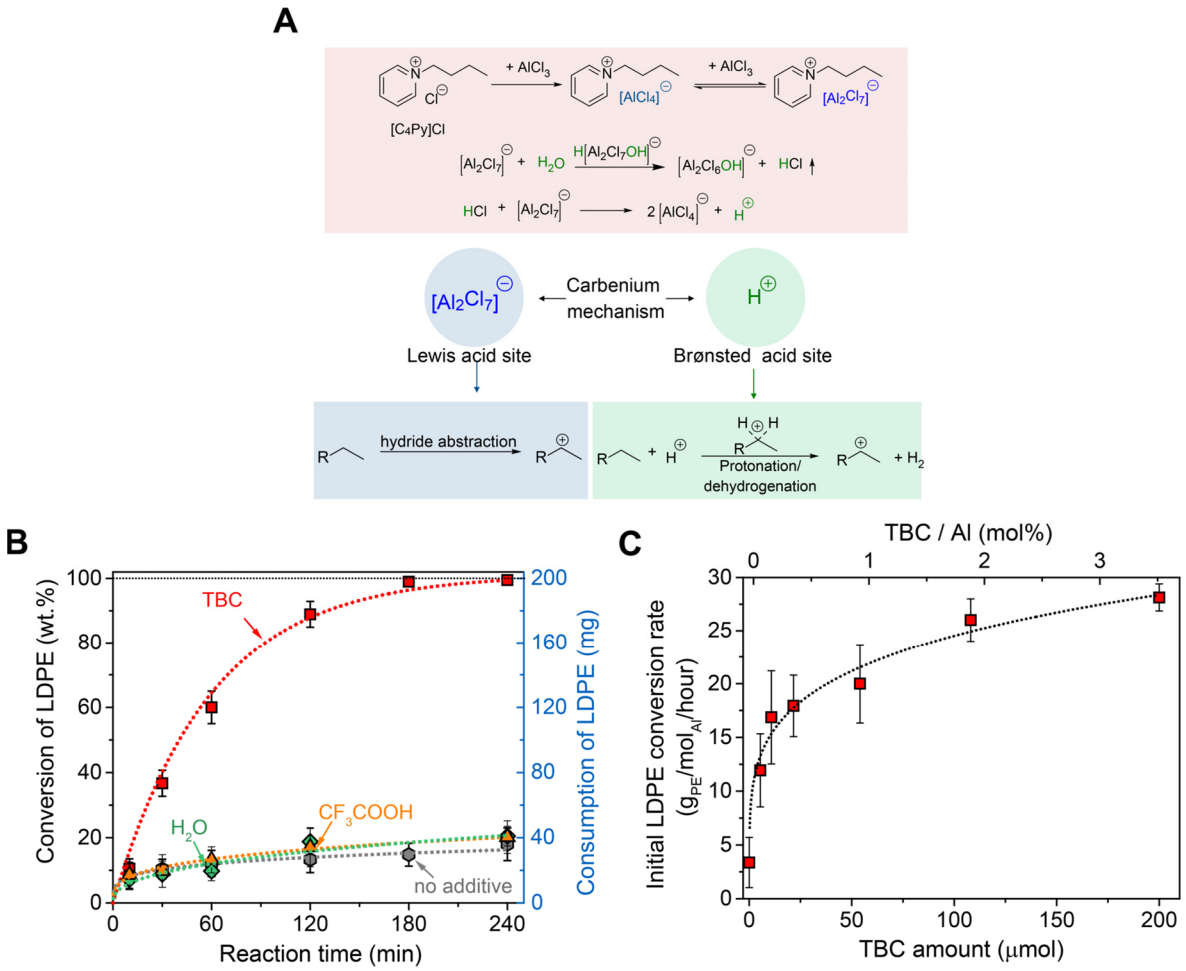

Fig. S9. Understanding the reaction pathways of tandem cracking-alkylation. (**A**) Illustration of the possible carbenium-ion mediated routes catalyzed by Lewis acid sites and Brønsted acid sites in [C_4Py]Cl-$AlCl_3$. (**B**) The influence of additives (H_2O, CF_3COOH and TBC) on the cracking-alkylation of LDPE and iC_5. Reaction conditions: LDPE 200 mg, isopentane (iC_5) 800 mg, [C_4Py]Cl-$AlCl_3$ 3 mmol, additive 0.05 mmol, DCM 3 mL, 70 °C. (**C**) Initial LDPE conversion rate plotted against TBC amount varying from 5 μmol to 200 μmol. Note that the initial LDPE conversion rate increased with an increase in TBC loading, confirming that the concentration of carbenium ions determines the reaction rate.

Supplementary Note. Lewis-acidic [C_4Py]Cl-$AlCl_3$ ionic liquids readily react with moisture to release HCl and may produce super acidic protons (Fig. S9A). Generally, Lewis acid-derived carbenium-ions are formed via hydride abstraction from a hydrocarbon. For Brønsted acid catalysis, carbenium ions are preferentially formed from olefins rather than from saturated hydrocarbons. The latter, however, undergoes protonation to form carbonium ions and then decomposes to a carbenium ion (see details in Fig. S5). Fig. S9B ruled out Brønsted acids and carbonium ions as the pathway because adding protic co-reagents (H_2O and CF_3COOH) did not change the reaction rates or the product distribution compared to [C_4Py]Cl-$AlCl_3$.

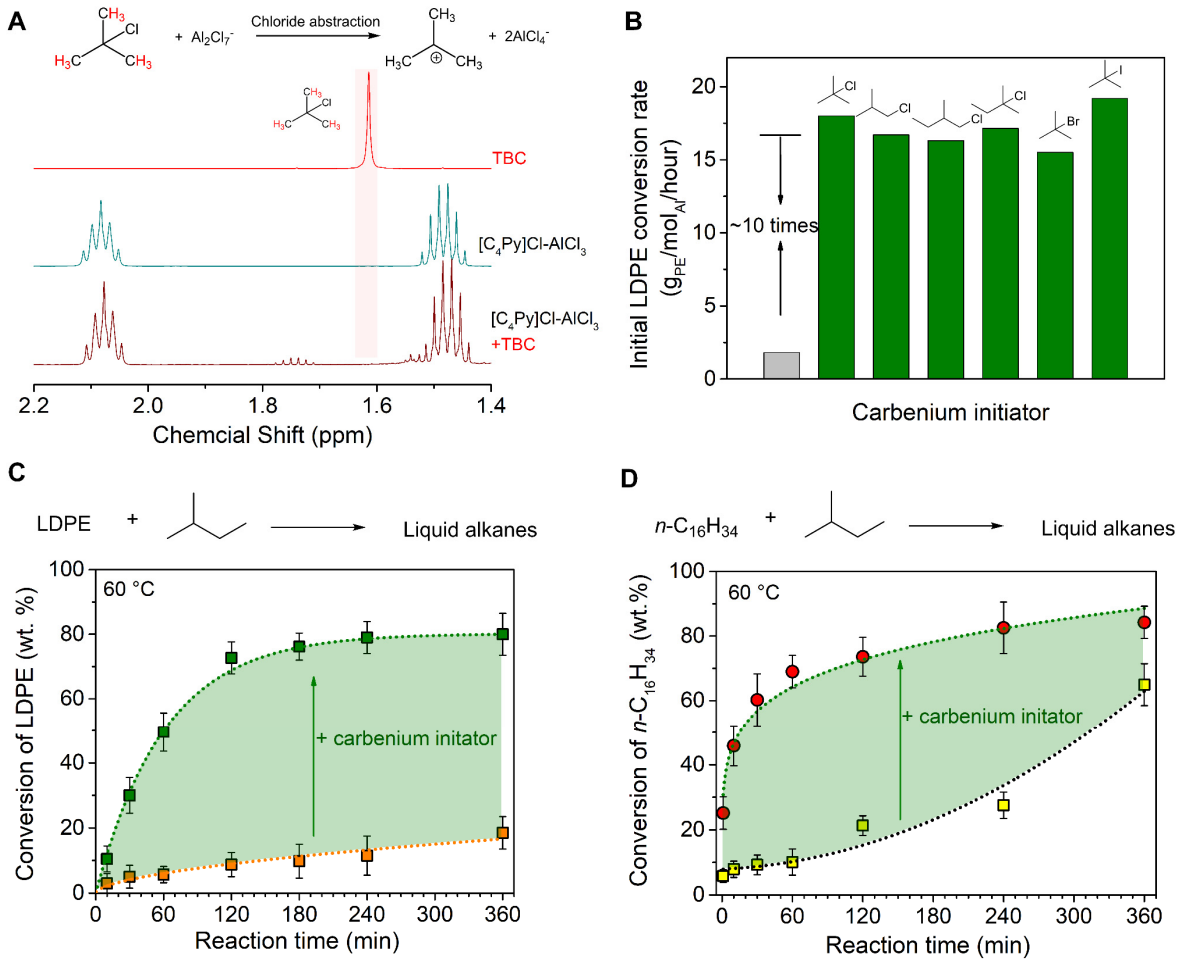

Fig. S10. Impact of carbenium ion initiator on the LDPE conversion. (**A**) Comparison of the ^{1}H NMR spectra of TBC, fresh [C4Py]Cl-AlCl3 catalyst, and the mixture of TBC in the [C4Py]Cl-AlCl3 catalyst. (**B**)The effect of various alkyl halide additives as carbenium ion initiators on the LDPE conversion rate over [C4Py]Cl-AlCl3 catalyst (alkyl halide additive: 1.5 mol% relative to [C4Py]Cl-AlCl3 loading). (**C-D**) The time-resolved conversion profile of LDPE and *n*-C16H34 in the presence and absence of TBC as carbenium ion initiator. Reaction conditions: LDPE/ *n*-C16H34 200 mg, isopentane (iC5) 800 mg, TBC 5 mg (0.05 mmol), [C4Py]Cl-AlCl3 3 mmol, DCM 3 mL, 60 °C.

Supplementary Note. Fig. S10A shows that the ^{1}H signal of TBC immediately disappeared after loading into the NMR tube and mixing with [C4Py]Cl-AlCl3 ionic liquid. This is attributed to the chloride abstraction from TBC to generate carbenium ions. A series of alkyl halides were tested as carbenium ion initiators (Fig. S10B). The reaction rate was at least one order of magnitude higher in the presence of the carbenium ion initiator than in its absence, indicating that the nature of the initiator did not influence the rate of reaction. The control experiments using *n*-hexadecane (*n*-C16H34) as a model for LDPE reacting with iC5 (Fig. S10, C and D) that substantiated the concentration of carbenium ion determines the reaction rate.

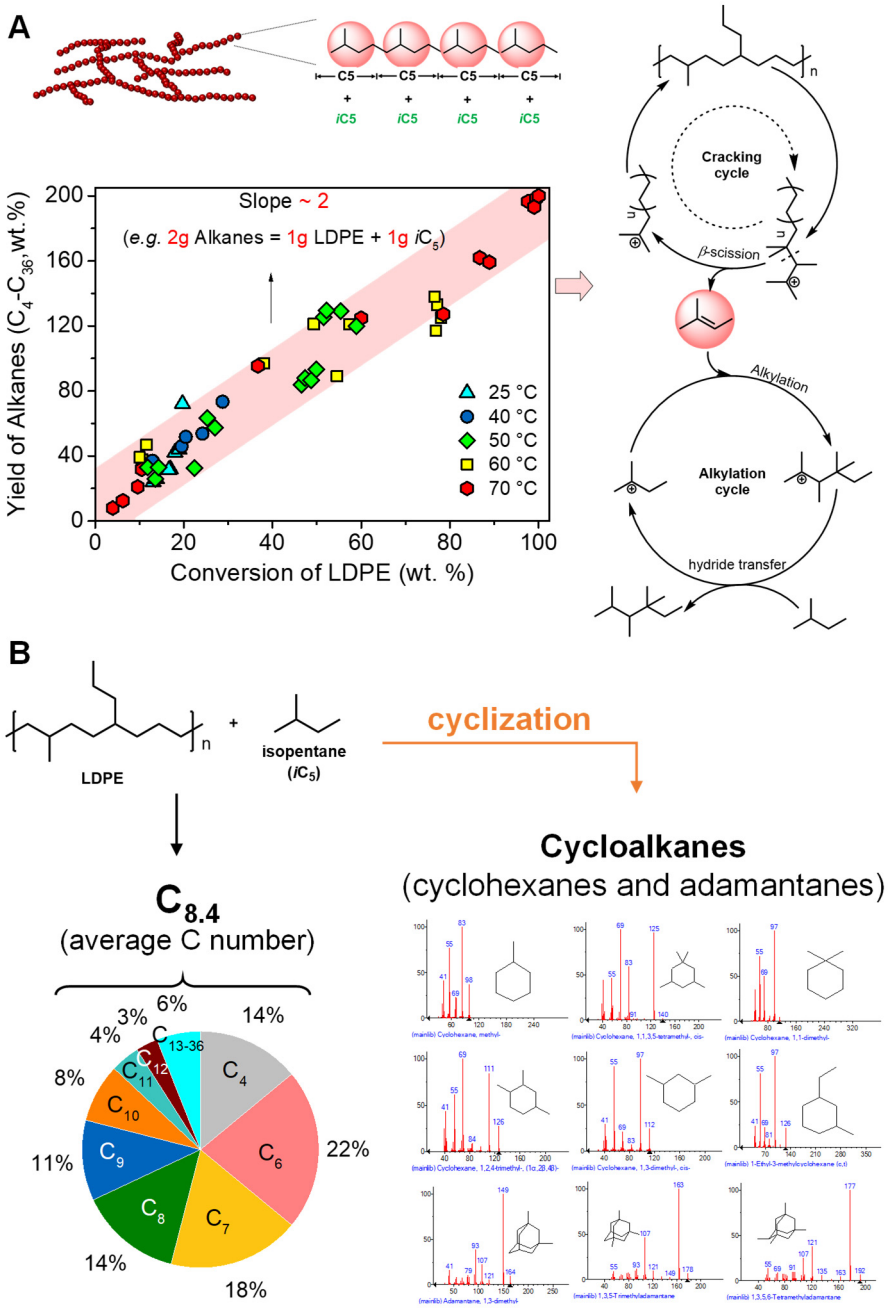

Fig. S11. (**A**)Tandem cracking-alkylation of LDPE with iC_5 showing the average size of the intermediately formed olefin is close to pentene, based on the ratio of molecular weight of the carbon products suggesting a ratio of converted LDPE and iC_5 to be approximately 1 : 1 in the reaction;(**B**) The competing cyclization pathway lead to the distribution of main products with average carbon atoms of ~8.4, which is lower than the theoretical value.

Supplementary Note. The mass yield of alkanes observed at different temperatures displayed a linear correlation with LDPE conversion with a slope of ~2.0, which is approximate twice the mass of LDPE converted. The LDPE, iC_5 and alkanes have the same chemical composition (C_nH_{2n+2}) such mass ratio equals a LDPE: iC_5 carbon number ratio of ca. 1 (Fig. S11A). This ratio indicates that the olefin intermediate from polyolefin cracking is pentene ($C_5^=$), which alkylates with iC_5 with a stoichiometric mass ratio of 1 to 1 (C_5H_{10} +

C_5H_{12}). This is the reason why iC_{10} is the proposed major cycle product (depicted in Figure 2). Actually, the distribution of the main products is the branched alkanes with average carbon atoms of ~8.4, which is lower than the theoretical value of 10 ($C_{10}H_{22}$). The lower carbon production represents higher H/C ratios, which means that the competing cyclization occurs and subsequent hydride/methyl shifts that yield polycyclic alkanes and red oil with decreased H/C ratios. Evidently, we detected the cyclohexanes and adamantanes as by-products (Fig. S11B), which agree well with this trend. Notably, the observation is also in good agreement with our published data in the liquid alkylation of iC_4 with butane deviating from the theoretical carbon number and H/C ratio (*21*).

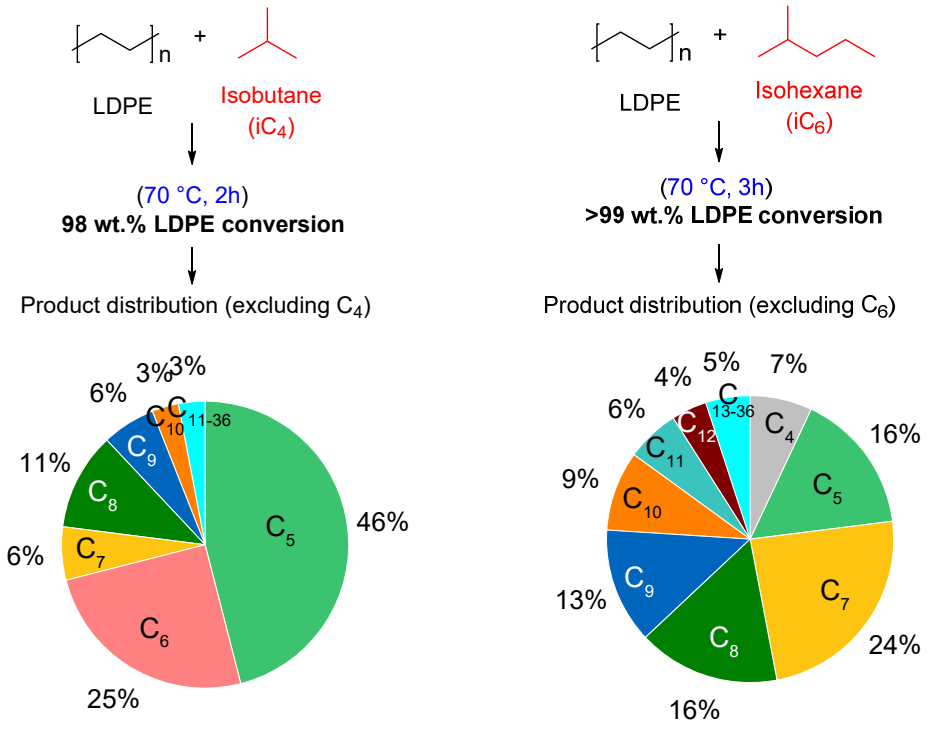

Fig. S12. Cracking-alkylation of LDPE with *i*C_4 and *i*C_6 as co-reactant under optimal conditions, giving nearly quantitatively LDPE conversion and branched alkanes. Reaction conditions of the iC_4-involved system: LDPE 1 g, isobutane (*i*C_4) 4 g, [C_4Py]Cl-$AlCl_3$ 15 mmol, additive 0.25 mmol, DCM 15 mL, 70 °C, 2 h, 2 MPa (N_2); reaction conditions for *i*C_6 -involved systems: LDPE 200 mg, *i*C_6 800 mg, [C_4Py]Cl-$AlCl_3$ 3 mmol, TBC 0.05 mmol, dichloromethane (DCM) 3 mL, 70 °C.

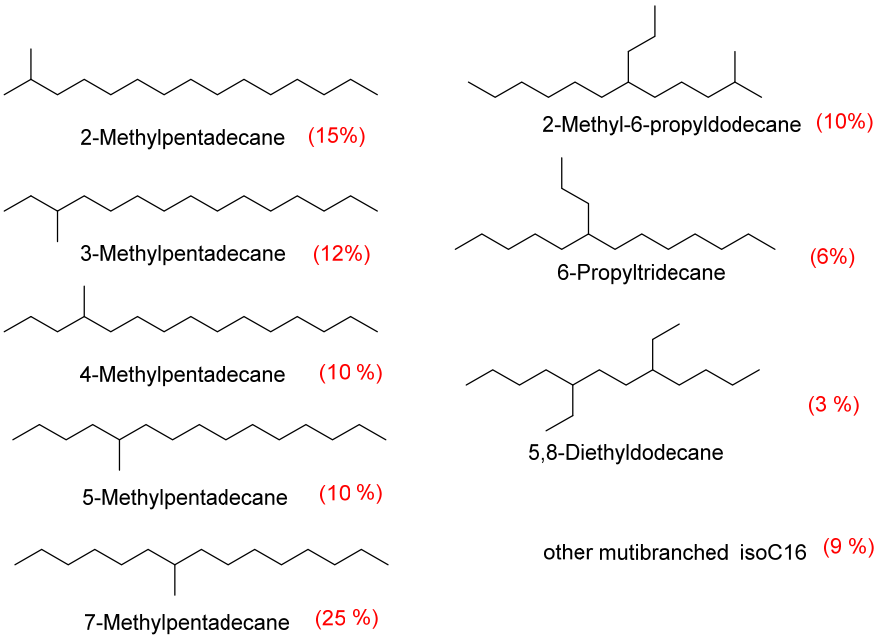

Fig. S13. Fraction of C_{16} isomers in the tandem cracking-alkylation of *n*-hexadecane ($nC_{16}H_{34}$) at a low conversion (~5 %). All compounds were identified by GC-MS.

Supplementary Note. To understand the cleavage pathways, control experiments were carried out using *n*-hexadecane ($nC_{16}H_{34}$) as a model for LDPE reacting with iC_5. At a low conversion (~5 %), the main products were the C_{16} isomers reaching 70%, in which the monomethyl isomers are dominated. This indicates that the skeletal isomerization of linear paraffin to branched alkanes occurs more rapidly than cracking. The thermodynamic calculation showed that the isomerization is slightly exergonic [ΔGr^o (70 °C) ≈ -8 kJ/mol, see Fig. S1], preferentially forming more stable tertiary carbenium ions. As a consequence, the cracking of carbenium ions occurs once the paraffin isomerized, and increases with its branching degree (Type A > Type B > Type C >> Type D). This can explain why monobranched C_{16} isomers were dominant at the initial stage, direct β-scission of monobranched carbocations hardly occurs due to the higher formation energy of primary carbenium.

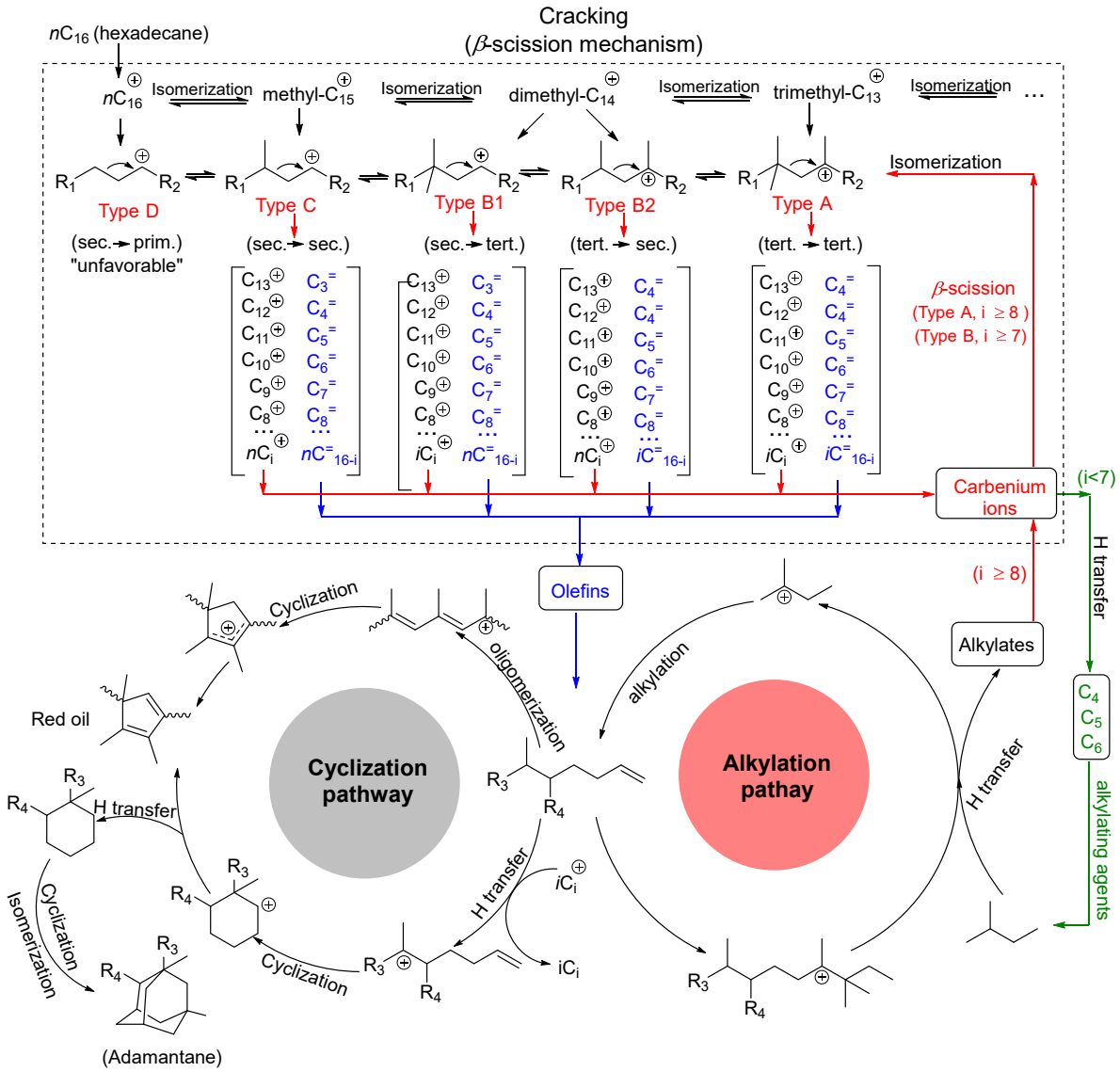

Fig. S14. Schematic illustration of the proposed reaction pathways for the cracking of *n*-hexadecane ($nC_{16}H_{34}$), combined with iC_5-free and iC_5-involved secondary reactions including isomerization, alkylation, cyclization and oligomerization.

Supplementary Note. The evolution of the products of LDPE deconstruction is in accordance with a consecutive mechanism using $nC_{16}H_{34}$ as an example. The inititation will produce a secondary carbenium (nC_{16}^{+}), followed by rapid isomerization via consecutive hydride- and methyl-shifts to produce stable *tert*-carbenium ions. Besides, the increase of the branching degree (linear →monobranched → dibranched→ tribranched) is faster than its decrease via reverse reactions (*27*). Simultaneously, a set of formed carbenium ions further crack via *β*-scission, in which the degree of branching determines the mode of *β*-scission. The relative rates decrease as follows: Type A > Type B > Type C >> Type D (see details in Fig. S6). Thus, the skeletal isomerization reactions occur initially, preferentially forming the energetically more-favorable branched *tert*-carbenium ions that undergo type A *β*-scission. Next, alkenes formed in the cracking process react in the alkylation cycle via addition to carbenium ions generated from iC_5. The kinetically and thermodynamically coupling of the

exothermic C-C bond cleavage with alkylation drives the reaction forward and enables complete conversion at low temperatures. While in the absence of iC_5, olefins can either undergo oligomerization to form red oil, or proceed with an intermolecular hydride transfer to obtain unsaturated carbenium ions and a rapid cyclization in subsequent steps. We detected the cyclohexanes, adamantanes and ASO in our reaction agree well with this pathway.
It should be noted that the long-chain carbenium ions in the reaction systems can undergo further cracking, producing short alkenes and carbenium ions (e.g. $C_{4,5,6}$). Besides being an alkylation agent to alkylate again, these short $C_{4,5,6}$ carbenium ions can also abstract a hydride from another alkane or polymer to produce corresponding $C_{4,5,6}$ alkanes. This is the reason why light isoalkanes (C_4-C_6) are always produced. In practice, the light isoalkanes formed in this process and unreacted isopentane can be used together as alkylation agents, allowing them to operate to a large extent self-sufficiently.

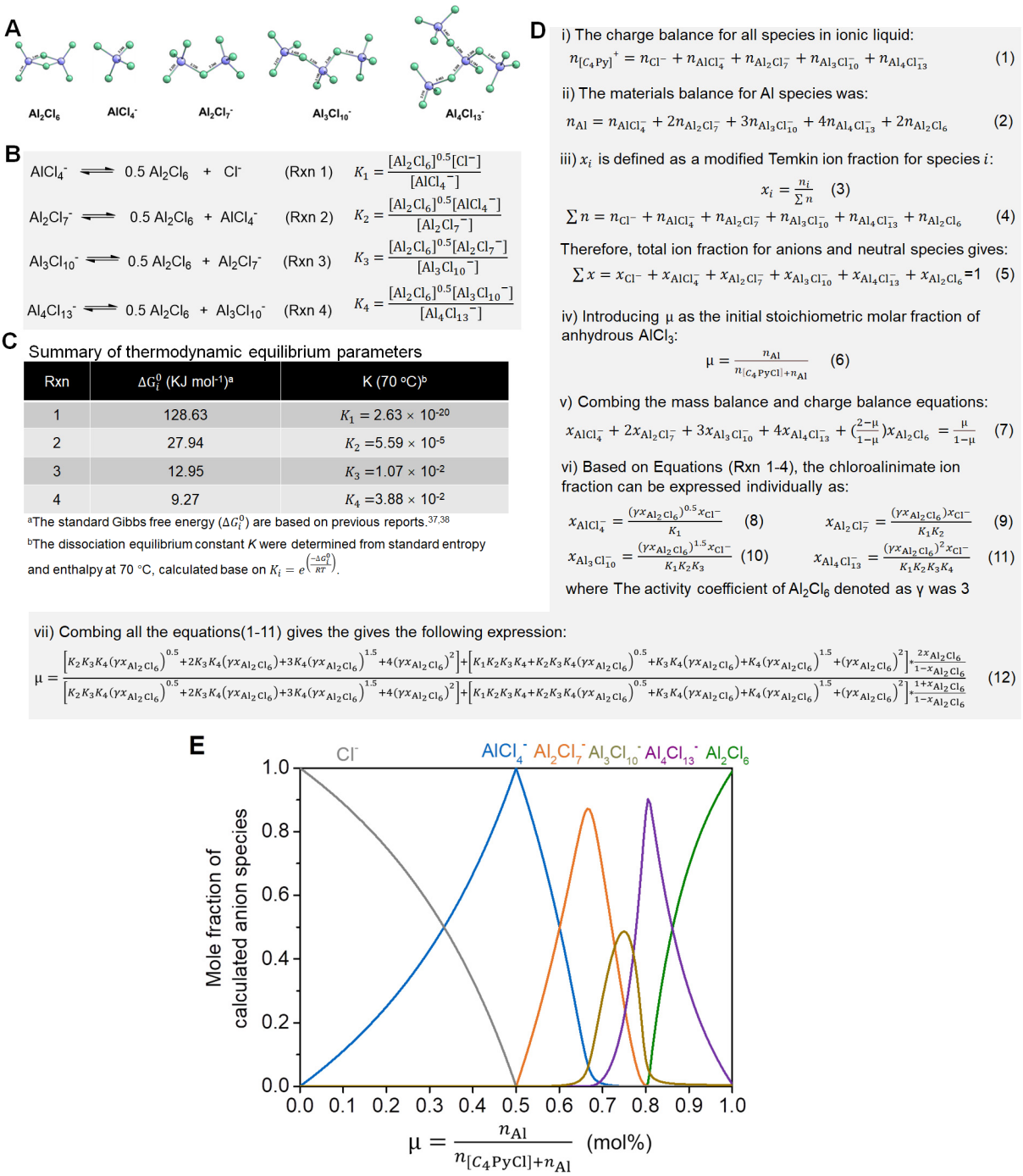

Fig. S15. Thermodynamic calculations of chloroaluminate speciation. (**A**)Typical chloroaluminate speciation of the [C4Py]Cl-AlCl3 ionic liquid, including the anhydrous aluminum chloride (exists as dimer Al_2Cl_6) and chloroaluminate anions ($AlCl_4^-$, $Al_2Cl_7^-$, $Al_3Cl_{10}^-$ and $Al_4Cl_{13}^-$). **(B)** The formation of chloroaluminate species follows the four equilibrium equations with the respective equilibrium constants. (**C**) The summary of the thermodynamic equilibrium parameters, including the standard Gibbs free energy (ΔG_i^0) and corresponding equilibrium constant at 70 °C. (**D**) Derivation of various chloroaluminate fractions as a function of the initial stoichiometric molar fraction of anhydrous aluminum chloride (μ). (**E**) Calculated concentrations of chloroaluminate anions plotted against the

molar fraction of anhydrous aluminum chloride (μ was in the range of 0 and 1 at interval 0.005) at 70 °C. All data were calculated based on equations 1-12 (Fig. S15D) using Python.

Supplementary Note. The nature of chloroaluminate anions closely depends on the molar fraction of aluminum chloride. Anhydrous aluminum chloride (Al_2Cl_6) reacts with *N*-butyl pyridinium chloride, yielding various negatively charged chloroaluminate species, including $AlCl_4^-$, $Al_2Cl_7^-$, $Al_3Cl_{10}^-$ and $Al_4Cl_{13}^-$ (their DFT-optimized structures are shown in Fig. S15A). These chloroaluminate anions are interrelated according to equilibria shown in Rxn1-4 (Fig. S15B). The corresponding thermodynamic parameters are summarized in Fig. S15C according to previous reports, including the standard enthalpy (ΔH_i^0) and entropy (ΔS_i^0) as well as equilibrium constants (*37, 38*). Considering the charge balance and mass balance of all species in the ionic liquid, the concentration of various chloroaluminate species can be represented by the function of the initial stoichiometric molar fraction of anhydrous aluminum chloride (denoted as μ), the detailed derivations are shown in Fig. S15D.
We calculated the composition of ionic liquid and plotted the chloroaluminate concentrations against the molar fraction of anhydrous aluminum chloride. As shown in Fig. S15E, the ionic liquid with a low aluminum chloride fraction ($\mu \leq 0.5$) only presents a mononuclear $AlCl_4^-$ anion, in which the four chloride ligands around the Al center render it chemically inert. Increasing aluminum chloride fraction further results in the formation of dimeric $Al_2Cl_7^-$ anions, which reached the maximum of ~90 % at $\mu = 0.67$ (*i.e.*, the molar ratio of $AlCl_3$ to $[C_4Py]Cl = 2:1$). Polymeric chloroaluminate anions ($Al_3Cl_{10}^-$ and $Al_4Cl_{13}^-$) become predominant dominant at high fractions of aluminum chloride ($\mu > 0.67$) and equilibrated with solid aluminum chloride resulted in a slurry phase (*39*). Therefore, we focused on the homogenous $[C_4Py]Cl$-$AlCl_3$ ionic liquids with the aluminum chloride loading in the range of 0.5 to 0.67 ($0.5 \leq \mu \leq 0.67$) for polyolefin catalysis, in which monomeric $AlCl_4^-$ and dimeric $Al_2Cl_7^-$ dominate.

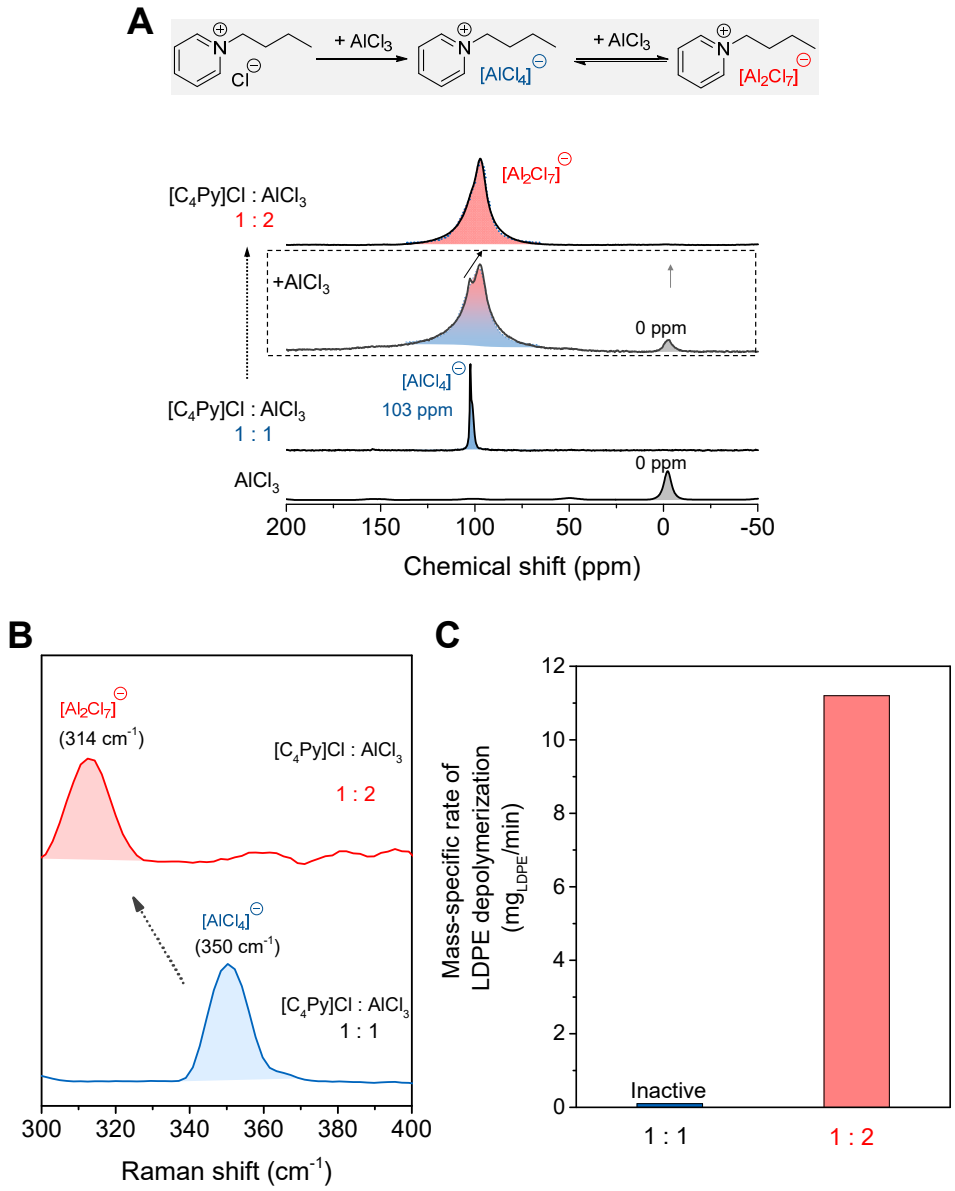

Fig. S16. **Summary of chloroaluminate speciation and catalytic activity.** (**A**) *In situ* ^{27}Al MAS NMR spectroscopy on [C4Py]Cl-AlCl3 at room temperature with anhydrous AlCl3 to [C4Py]Cl ratio of 1:1 and 1:2, compared with the pure AlCl3. (**B**) Raman spectra of [C4Py]Cl-AlCl3 catalysts with anhydrous AlCl3 to [C4Py]Cl ratio of 1:1 and 1:2. (**C**) Comparison of mass-specific LDPE conversion rate over two [C4Py]Cl-AlCl3 catalysts (1:1 vs. 1:2). Reaction conditions: LDPE 200 mg, isopentane (*i*C5) 800 mg, [C4Py]Cl-AlCl3 loading 3 mmol, TBC 0.2 mmol, DCM 3 mL, temperature 70 °C.

Supplementary Note. We resorted to *in situ* ^{27}Al MAS NMR to interrogate the formation of specific species (i.e., the $AlCl_4^-$ and $Al_2Cl_7^-$) as a function of the molar ratio between AlCl3 and [C4Py]Cl (Fig. S16A) (*34, 40*). When anhydrous AlCl3 and [C4Py]Cl were loaded into the NMR rotor (in a molar ratio of 1:1), AlCl3 was immediately converted to $AlCl_4^-$ anions, which have a resonance peak at 103 ppm at room temperature (*41*). Increasing the molar ratio of AlCl3 /[C4Py]Cl to 2:1 resulted in a broad peak, which is assigned to $Al_2Cl_7^-$ anions (*42*).

The Raman characterization (Fig. S16B) also upholds the ^{27}Al MAS NMR results. The Raman spectrum of the $[C_4Py]Cl$-$AlCl_3$ (1:1) showed a characteristic peak at 350 cm^{-1} corresponding to the $AlCl_4^-$. A new signal was observed at 314 cm^{-1} ($[C_4Py]$ Cl: $AlCl_3$= 1:2), which can be assigned to the $Al_2Cl_7^-$ anions (*43-45*). Increasing the initial fraction of anhydrous aluminum chloride promotes the transformation from $AlCl_4^-$ to $Al_2Cl_7^-$, which in turn results in improved reaction rates (Fig. S16C).

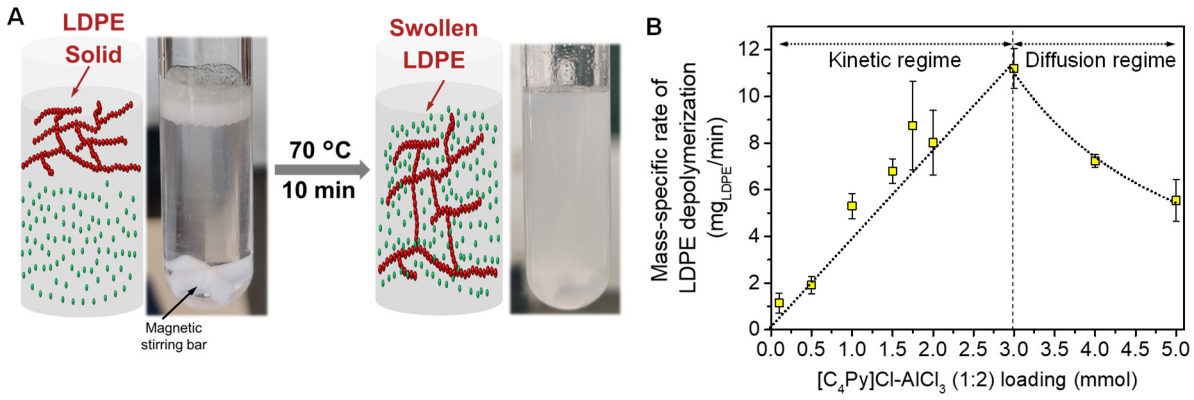

Fig. S17. **Kinetically controlled regime on the cracking-alkylation of LDPE with iC$_5$.** (**A**) Snapshot of Swollen LDPE during the reaction with low ionic liquid loading of 0.5 mmol (70 °C, 10 min). Dichloromethane is used to bridge the solubility of isopentane and the ionic liquid, enabling an expanded surface where the catalyst and polymer interact. (**B**) Plot for the correlation between the mass-specific activity of LDPE depolymerization on [C$_4$Py]Cl-AlCl$_3$ ionic liquid loading. (Note: we studied the rates at low conversions < 20 wt.%, and the carbon balances were >95 %). Reaction conditions: LDPE 200 mg, isopentane (*i*C$_5$) 800 mg, [C$_4$Py]Cl-2AlCl$_3$ 0.1-5 mmol, TBC 0.2 mmol, DCM 3 mL, temperature 70 °C.

Supplementary Note. The C-C cleavage of polyolefins over heterogeneous solid catalysts presents a more challenging hurdle than that of small hydrocarbons, due to polymer recalcitrance by limiting chain mobility and accessibility to catalytic sites. Most of the deconstruction reactions, therefore, show a remarkable enhancement of the reaction via liquefying polymer, albeit mass transfer effects cannot be ruled out completely owing to the high viscosity. Especially in tandem catalysis over diverse catalytic functions, the distant spacing of its different kinds of sites limiting the contact of polymer strands with catalytically active sites retards the reaction. Our cracking-alkylation strategy proceeds using room-temperature molten chloroaluminate salts as the source for the catalytically active species, which are diluted in dichloromethane as mediating solvent to assure one-phase catalysis containing isopentane and swollen polymer strands, efficiently lowering the local mass-transfer limitations (Fig. S17A). We found that the mass-specific activities of LDPE depolymerization varied the ionic liquid concentration (See Fig. S17B), which showed a linear correlation with the [C$_4$Py]Cl-AlCl$_3$ loading from 0.1 mmol to 3 mmol, indicating catalytic behavior under the kinetically controlled regime. Increasing the ionic liquid loading further did not improve the catalytic performance. The results suggested that the overloading of the ionic liquid triggers phase separation between LDPE/iC$_5$ and ionic liquid, resulting in the diffusion limitation retarded the reaction rate. Therefore, all the rates are measured under a kinetically controlled regime.

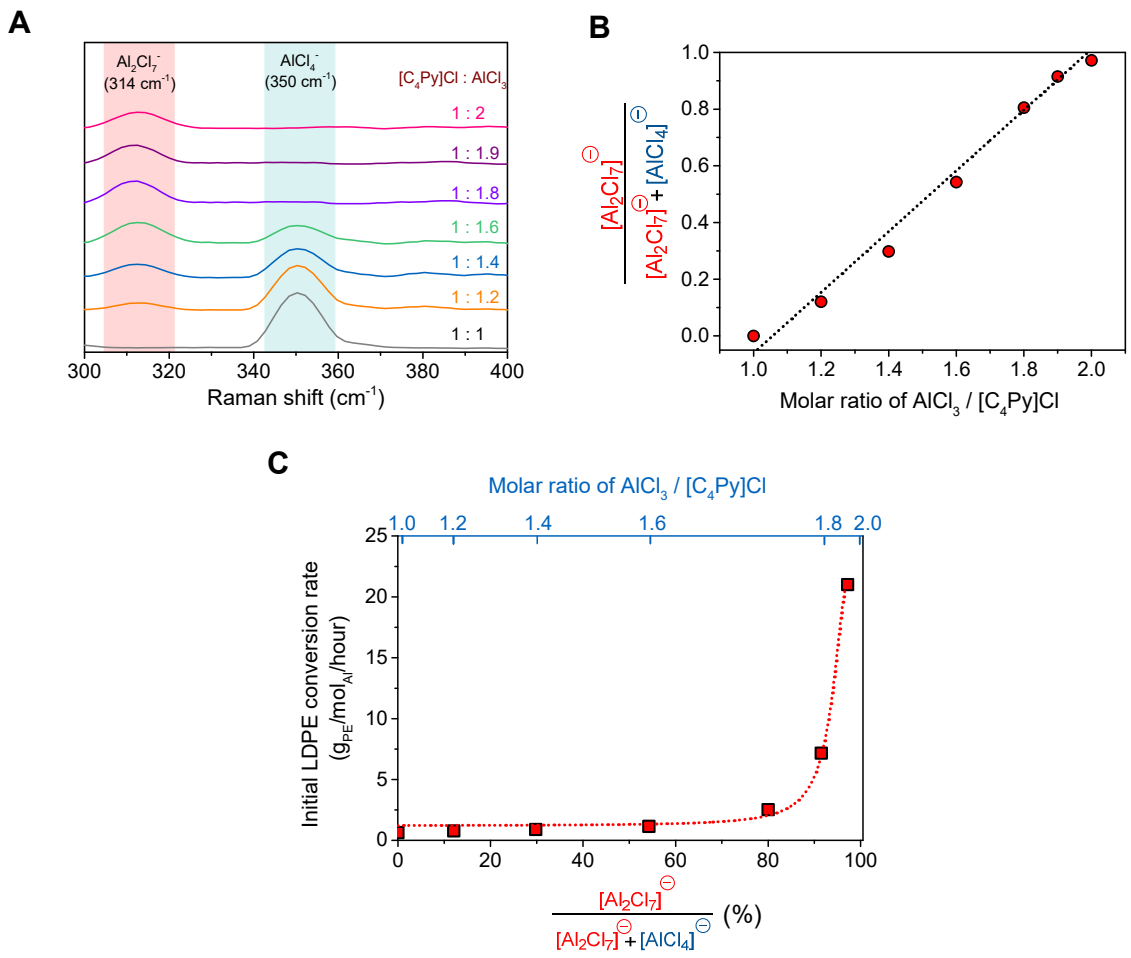

Fig. S18. **The chloroaluminate anions governing the activity.** (**A**)Raman spectra of $[C_4Py]Cl$-$AlCl_3$ ionic liquids with the varying molar ratio of $AlCl_3$ and $[C_4Py]Cl$. (**B**) Plot of fraction of $Al_2Cl_7^-$ anions ($Al_2Cl_7^-/[AlCl_4^- + Al_2Cl_7^-]$) versus the molar ratio of $AlCl_3$/ $[C_4Py]Cl$. Note: the ratio of the Raman scattering cross-sections of $AlCl_4^-$ and $Al_2Cl_7^-$ were determined according to the previous reports (*46, 47*). (**C**) Comparisons of the initial conversion rate of LDPE over $[C_4Py]Cl$-$AlCl_3$ ionic liquids with varying molar fraction of $Al_2Cl_7^-$ ($Al_2Cl_7^-/(AlCl_4^- + Al_2Cl_7^-)$). (Reaction conditions: LDPE/iC_5 = 1/3, DCM 3 mL, 70 °C, 5 mg TBC as additive).

Supplementary Note. Fig. S18A shows that the $Al_2Cl_7^-$ signal gradually increased as the molar ratio of $AlCl_3$ to $[C_4Py]Cl$ increased, accompanied by a decrease in the monomeric $AlCl_4^-$ signal. The ratio of $Al_2Cl_7^-$ and ($AlCl_4^- + Al_2Cl_7^-$) was proportional to the molar ratio of $AlCl_3$ to $[C_4Py]Cl$ (Fig. S18B). We plotted the initial LDPE conversion rate against the ratio of $Al_2Cl_7^-/(AlCl_4^- + Al_2Cl_7^-)$, showing that $[C_4Py]Cl$-$AlCl_3$ with nearly 100% $Al_2Cl_7^-$ anions gave a much higher initial conversion rate compared with the other samples. For instance, the $[C_4Py]Cl$-$AlCl_3$ (1:2) showed 14 times more activity than the $[C_4Py]Cl$-$AlCl_3$ (1:1.8) even with 90% $Al_2Cl_7^-$ anions (Fig. S18C).

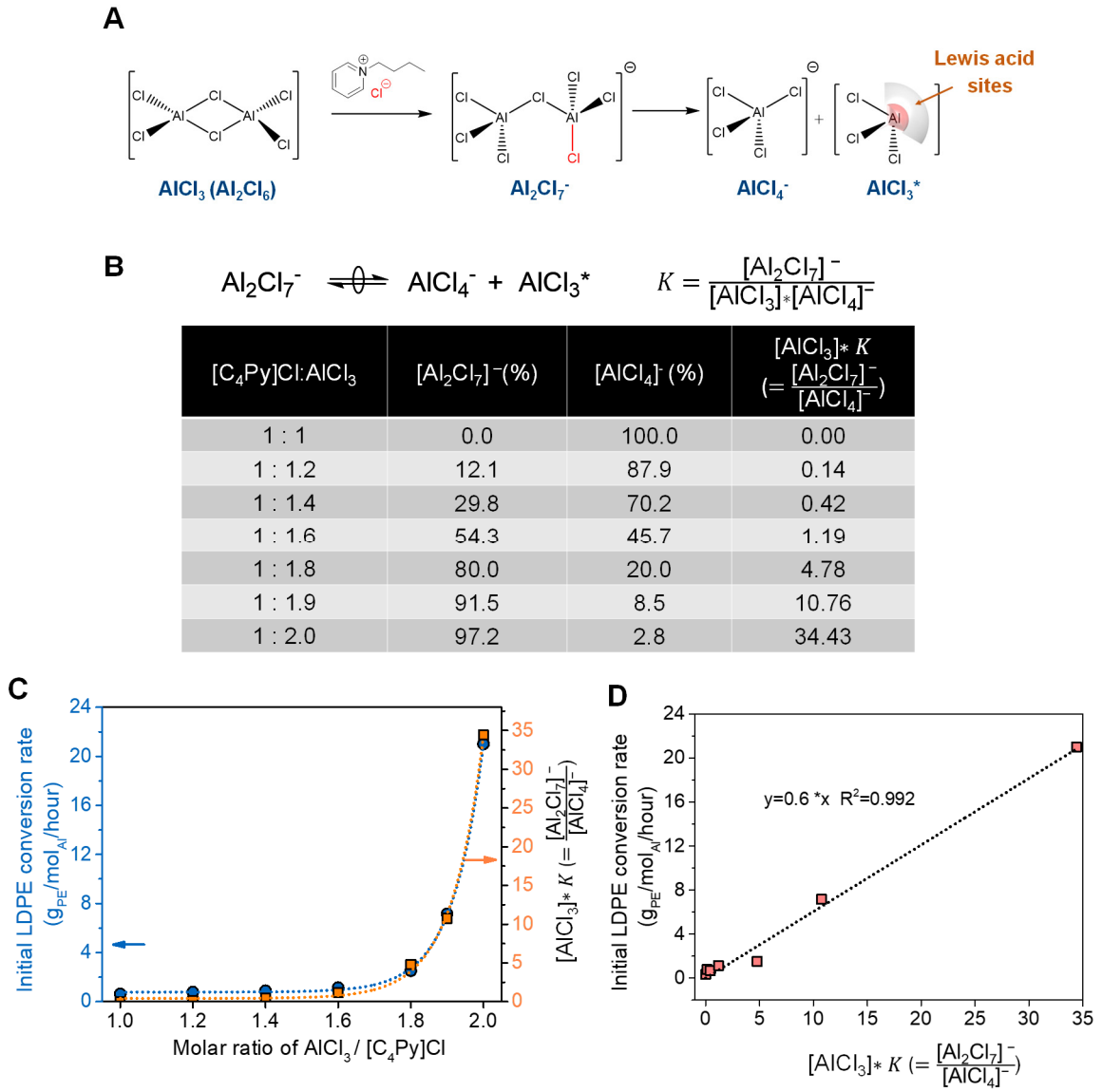

[C4Py]Cl:AlCl3	[Al2Cl7]-(%)	[AlCl4]- (%)	[AlCl3]* K (= [Al2Cl7]- / [AlCl4]-)
1 : 1	0.0	100.0	0.00
1 : 1.2	12.1	87.9	0.14
1 : 1.4	29.8	70.2	0.42
1 : 1.6	54.3	45.7	1.19
1 : 1.8	80.0	20.0	4.78
1 : 1.9	91.5	8.5	10.76
1 : 2.0	97.2	2.8	34.43

Fig. S19. Kinetic analysis uncovers catalytically active sites derived from the dissociation of $Al_2Cl_7^-$ (**A**) Schematic of the formation of active $AlCl_3$* species via dissociation of the dimeric $Al_2Cl_7^-$, and showing a dissociated equilibrium among monomeric $AlCl_4^-$, $AlCl_{3*}$ and $Al_2Cl_7^-$ (K: equilibrium constant). (**B**) Summary of the molar fraction of $AlCl_4^-$ and $Al_2Cl_7^-$ calculated from Raman analysis in Fig. S18, and corresponding $AlCl_3$* concentration determined by the dissociation equilibrium. (**C**) Relationship between initial LDPE conversion rate, empirical [$AlCl_3$] concentration (K×[$AlCl_3$*]), and the molar ratio of $AlCl_3$ to [C_4Py]Cl. (**D**) Initial LDPE conversion rate plotted against empirical [$AlCl_3$] concentration (K*[$AlCl_3$]).

Supplementary Note. Anhydrous aluminum chloride has a covalent structure and is present as a dimer (Al_2Cl_6, Fig. S19A). Adding organic chloride salt (N-pyridinium chloride,) Al_2Cl_6 accepts a chloride to form negatively charged Al species, heptachloroaluminate $Al_2Cl_7^-$ (*48*). Due to an easily broken chloride bridge, the dimeric $Al_2Cl_7^-$ dissociates transiently into a

coordinatively saturated inert $AlCl_4^-$ and an active $AlCl_3$* featuring Lewis acidity. The $AlCl_3$* concentration can be expressed as (Fig. S19B),

$[AlCl_3] = \frac{[Al_2Cl_7]^-}{[AlCl_4]^-} * K$, where K is the equilibrium constant.

Interestingly, we found that the initial reaction rate of $[C_4Py]Cl$-$AlCl_3$ is proportional to the molar ratio of $AlCl_3$/$[C_4Py]Cl$, in close correlation with the dissociated $AlCl_3$* concentration (Fig. S19C). We, therefore, attribute the reactivity enhancement to the increased $AlCl_3$* concentration from dimeric $Al_2Cl_7^-$ anions. To better understand this trend, we plotted the turnover frequencies of $[C_4Py]Cl$-$AlCl_3$ against the $AlCl_3$* concentration (Fig. S19D), which showed a linear correlation. Thus, increasing the molar ratio of $AlCl_3$ to $[C_4Py]Cl$ can increase the ratio of dimeric $[Al_2Cl_7]^-$ species, which in turn results in the increased $[AlCl_3]$ active species, improving overall activity for cracking-alkylation.

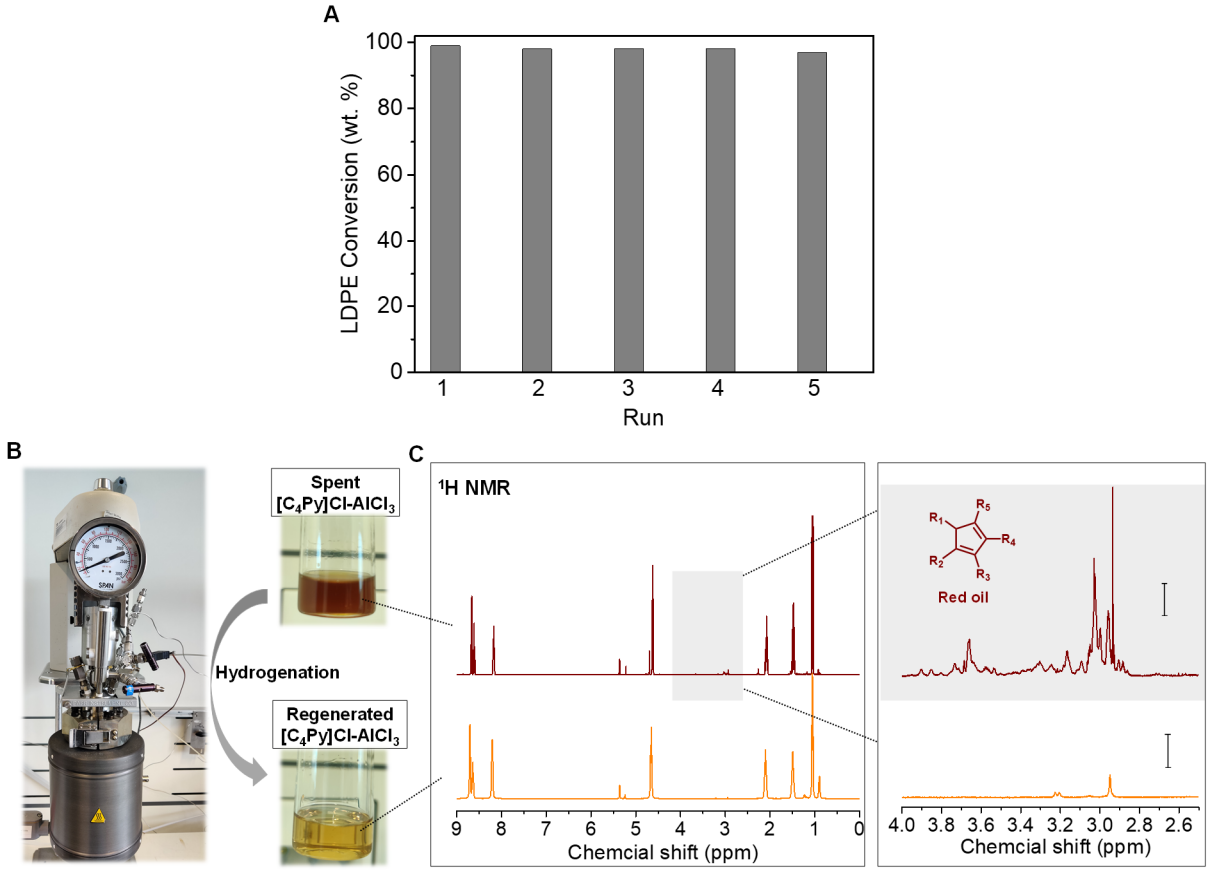

Fig. S20. Repeated batch experiments and catalyst regeneration. (**A**) Repeated batch tests of catalytic LDPE upcycling into liquid alkanes over [C_4Py]Cl-$AlCl_3$. Initial reaction conditions: LDPE 5 g, initial light paraffin pool 20 g (C_4: 40 wt.%, C_5: 40 wt.%, C_6: 20wt. %), [C_4Py]Cl-$AlCl_3$ 30 mmol, TBC 100 mg, DCM 75 mL, 2 MPa (N_2), 70 °C, 2 h. In each repeated run, 5 g of LDPE powder and 4 g of light paraffin refilling in the 300 mL autoclave. The [C_4Py]Cl-$AlCl_3$ catalyst retained its activity and can be used without regeneration at least five times, constantly reaching full LDPE conversion. (**B**) Regeneration of spent [C_4Py]Cl-$AlCl_3$ via H_2 hydrogenation over Pd/C catalyst, 180 °C, 2 MPa H_2, 4 h, following the procedure reported by Li et al (*49*). (**C**) ^{1}H NMR spectra of spent [C_4Py]Cl-$AlCl_3$ and regenerated [C_4Py]Cl-$AlCl_3$ after hydrogenation, suggesting that red oil can be converted into saturated hydrocarbons via hydrogenation.

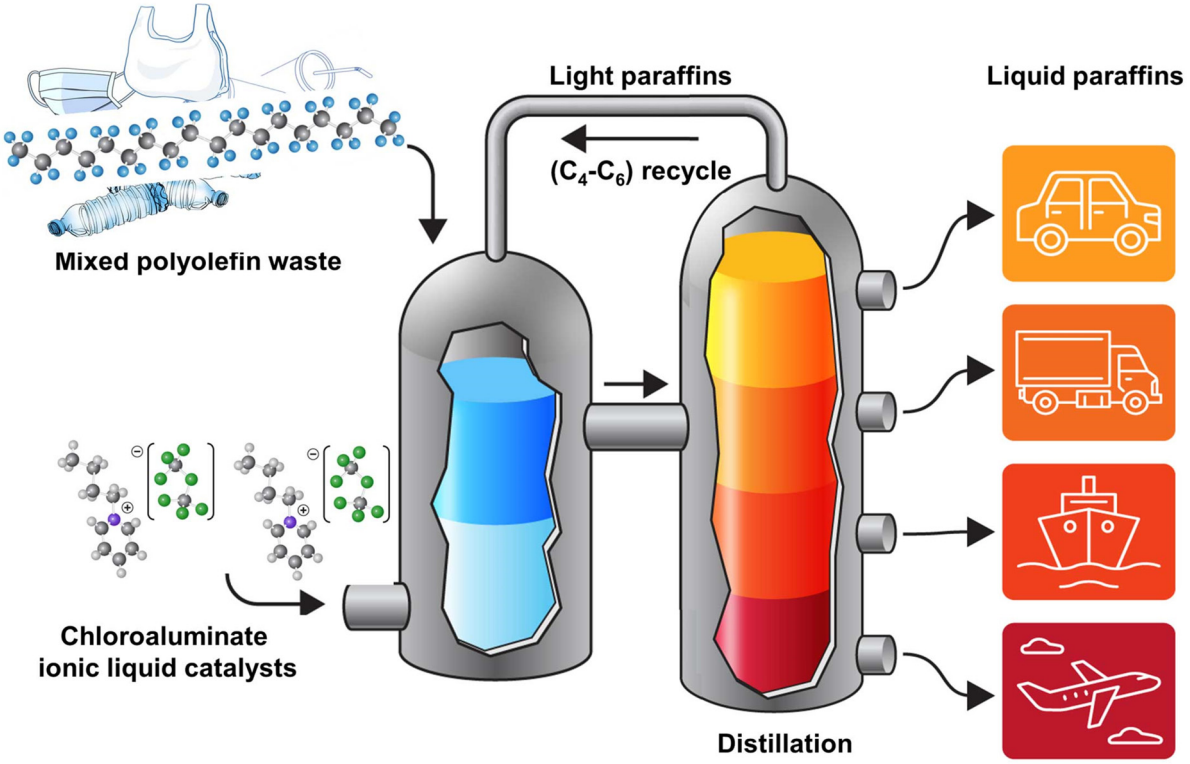

Fig. S21. Conceptual process diagram for catalytic upcycling of postconsumer polyolefin waste via tandem cracking-alkylation process to produce liquid fuels over chloroaluminate ionic liquid.

Supplementary Note. The ionic liquids catalyst technologies offer potential advantages due to the negligible vapor pressure, non-inflammability, high thermal stability, and a wide liquid-phase temperature range. Dichloromethane (DCM) dilutes the ionic liquid, lowering the viscosity and the local mass-transfer barriers. DCM is, however, fully recycled via the top of the distillation product slate including all light products.

Excess of isopentane to polyolefin ratios: It should be emphasized that the ratio between lite alkanes (isopentane) and polyolefin was 4, which is by far lower than the excess of iso-alkanes in the current industrial alkylation process. The latter typically needs practically large excesses of isoparaffins over alkenes ($n_{isoparaffins}$:$n_{alkenes}$ 7-10) to minimize the formation of red oil via oligomerization (*27*). These side reactions occur because the rate-limiting hydride transfer step in alkylation is significantly slower than the oligomerization of the alkenes. In our case, the synchronous release of alkenes via cracking in the presented cascade cracking-alkylation retards the olefin addition to the mixture and allows so a better control on product distribution and minimizes the formation of the red oil waste product. Judged by the current state of first-generation catalysts the strategy could allow to use polyolefins directly as potential feed in the refinery.

Notably, the upcycling process requires the addition of isopentane only for the start. Subsequently, the light isoalkanes (C_4-C_6) formed in this process and unreacted isopentane can be used together as alkylation reaction partners, allowing to operate to a large extent self-sufficiently, enabling full conversions of the recycle (this is possible as methane, ethane, and propane are hardly produced). We are convinced that this is an economically more promising approach for a decentralized conversion than the higher temperature processes, especially given the compatibility with existing infrastructure in many modern refineries.

References and Notes

1. R. Geyer, J. R. Jambeck, K. L. Law, Production, use, and fate of all plastics ever made. *Sci. Adv.* **3**, e1700782 (2017). doi:10.1126/sciadv.1700782 Medline

2. J. M. Garcia, M. L. Robertson, The future of plastics recycling. *Science* **358**, 870–872 (2017). doi:10.1126/science.aaq0324 Medline

3. G. W. Coates, Y. D. Y. L. Getzler, Chemical recycling to monomer for an ideal, circular polymer economy. *Nat. Rev. Mater.* **5**, 501–516 (2020). doi:10.1038/s41578-020-0190-4

4. S. C. Kosloski-Oh, Z. A. Wood, Y. Manjarrez, J. P. de Los Rios, M. E. Fieser, Catalytic methods for chemical recycling or upcycling of commercial polymers. *Mater. Horiz.* **8**, 1084–1129 (2021). doi:10.1039/D0MH01286F Medline

5. Z. O. G. Schyns, M. P. Shaver, Mechanical recycling of packaging plastics: A review. *Macromol. Rapid Commun.* **42**, e2000415 (2021). doi:10.1002/marc.202000415 Medline

6. S. M. Al-Salem, A. Antelava, A. Constantinou, G. Manos, A. Dutta, A review on thermal and catalytic pyrolysis of plastic solid waste (PSW). *J. Environ. Manage.* **197**, 177–198 (2017). doi:10.1016/j.jenvman.2017.03.084 Medline

7. A. J. Martín, C. Mondelli, S. D. Jaydev, J. Pérez-Ramírez, Catalytic processing of plastic waste on the rise. *Chem* **7**, 1487–1533 (2021). doi:10.1016/j.chempr.2020.12.006

8. I. Vollmer, M. J. F. Jenks, M. C. P. Roelands, R. J. White, T. van Harmelen, P. de Wild, G. P. van der Laan, F. Meirer, J. T. F. Keurentjes, B. M. Weckhuysen, Beyond mechanical recycling: Giving new life to plastic waste. *Angew. Chem. Int. Ed.* **59**, 15402–15423 (2020). doi:10.1002/anie.201915651 Medline

9. L. O. Mark, M. C. Cendejas, I. Hermans, The use of heterogeneous catalysis in the chemical valorization of plastic waste. *ChemSusChem* **13**, 5808–5836 (2020). doi:10.1002/cssc.202001905 Medline

10. G. Celik, R. M. Kennedy, R. A. Hackler, M. Ferrandon, A. Tennakoon, S. Patnaik, A. M. LaPointe, S. C. Ammal, A. Heyden, F. A. Perras, M. Pruski, S. L. Scott, K. R. Poeppelmeier, A. D. Sadow, M. Delferro, Upcycling single-use polyethylene into high-quality liquid products. *ACS Cent. Sci.* **5**, 1795–1803 (2019). doi:10.1021/acscentsci.9b00722 Medline

11. J. E. Rorrer, G. T. Beckham, Y. Román-Leshkov, Conversion of polyolefin waste to liquid alkanes with Ru-based catalysts under mild conditions. *JACS Au* **1**, 8–12 (2020). doi:10.1021/jacsau.0c00041 Medline

12. A. Tennakoon, X. Wu, A. L. Paterson, S. Patnaik, Y. Pei, A. M. LaPointe, S. C. Ammal, R. A. Hackler, A. Heyden, I. I. Slowing, G. W. Coates, M. Delferro, B. Peters, W. Huang, A. D. Sadow, F. A. Perras, Catalytic upcycling of high-density polyethylene via a processive mechanism. *Nat. Catal.* **3**, 893–901 (2020). doi:10.1038/s41929-020-00519-4

13. S. Liu, P. A. Kots, B. C. Vance, A. Danielson, D. G. Vlachos, Plastic waste to fuels by hydrocracking at mild conditions. *Sci. Adv.* **7**, eabf8283 (2021). doi:10.1126/sciadv.abf8283 Medline

14. X. Jia, C. Qin, T. Friedberger, Z. Guan, Z. Huang, Efficient and selective degradation of polyethylenes into liquid fuels and waxes under mild conditions. *Sci. Adv.* **2**, e1501591 (2016). doi:10.1126/sciadv.1501591 Medline

15. N. Morlanés, S. G. Kavitake, D. C. Rosenfeld, J.-M. Basset, Alkane cross-metathesis reaction between light and heavy linear alkanes, on a silica supported well-defined single-site catalyst. *ACS Catal.* **9**, 1274–1282 (2019). doi:10.1021/acscatal.8b02472

16. F. Zhang, M. Zeng, R. D. Yappert, J. Sun, Y.-H. Lee, A. M. LaPointe, B. Peters, M. M. Abu-Omar, S. L. Scott, Polyethylene upcycling to long-chain alkylaromatics by tandem hydrogenolysis/aromatization. *Science* **370**, 437–441 (2020). doi:10.1126/science.abc5441 Medline

17. D. P. Serrano, J. Aguado, J. M. Escola, Developing advanced catalysts for the conversion of polyolefinic waste plastics into fuels and chemicals. *ACS Catal.* **2**, 1924–1941 (2012). doi:10.1021/cs3003403

18. H. Yan, K. He, I. A. Samek, D. Jing, M. G. Nanda, P. C. Stair, J. M. Notestein, Tandem In_2O_3-Pt/Al_2O_3 catalyst for coupling of propane dehydrogenation to selective H_2 combustion. *Science* **371**, 1257–1260 (2021). doi:10.1126/science.abd4441 Medline

19. L. D. Ellis, N. A. Rorrer, K. P. Sullivan, M. Otto, J. E. McGeehan, Y. Román-Leshkov, N. Wierckx, G. T. Beckham, Chemical and biological catalysis for plastics recycling and upcycling. *Nat. Catal.* **4**, 539–556 (2021). doi:10.1038/s41929-021-00648-4

20. GlobalData, "Refinery alkylation units market installed capacity and capital expenditure (CapEx) forecast by region and countries including details of all active plants, planned and announced projects, 2022-2026," Report code GDGE1353ICR (2021).

21. A. Feller, I. Zuazo, A. Guzman, J. O. Barth, J. A. Lercher, Common mechanistic aspects of liquid and solid acid catalyzed alkylation of isobutane with n-butene. *J. Catal.* **216**, 313–323 (2003). doi:10.1016/S0021-9517(02)00068-4

22. N. Pfriem, P. H. Hintermeier, S. Eckstein, S. Kim, Q. Liu, H. Shi, L. Milakovic, Y. Liu, G. L. Haller, E. Baráth, Y. Liu, J. A. Lercher, Role of the ionic environment in enhancing the activity of reacting molecules in zeolite pores. *Science* **372**, 952–957 (2021). doi:10.1126/science.abh3418 Medline

23. L. Milaković, P. H. Hintermeier, Y. Liu, E. Baráth, J. A. Lercher, Influence of intracrystalline ionic strength in MFI zeolites on aqueous phase dehydration of methylcyclohexanols. *Angew. Chem. Int. Ed.* **60**, 24806–24810 (2021). doi:10.1002/anie.202107947 Medline

24. H. K. C. Timken, S. Elomari, S. Trumbull, R. Cleverdon, "Integrated alkylation process using ionic liquid catalysts," US Patent 7,432,408 (2008).

25. C. J. Adams, M. J. Earle, K. R. Seddon, Catalytic cracking reactions of polyethylene to light alkanes in ionic liquids. *Green Chem.* **2**, 21–24 (2000). doi:10.1039/a908167d

26. J. Estager, J. D. Holbrey, M. Swadźba-Kwaśny, Halometallate ionic liquids—Revisited. *Chem. Soc. Rev.* **43**, 847–886 (2014). doi:10.1039/C3CS60310E Medline

27. A. Feller, J. A. Lercher, in *Advances in Catalysis*, H. Knüpffer, Ed. (Academic Press, 2004), vol. 48, pp. 229–295.

28. A. S. Amarasekara, Acidic ionic liquids. *Chem. Rev.* **116**, 6133–6183 (2016). doi:10.1021/acs.chemrev.5b00763 Medline

29. S. Aschauer, L. Schilder, W. Korth, S. Fritschi, A. Jess, Liquid-phase isobutane/butene-alkylation using promoted Lewis-acidic IL-catalysts. *Catal. Lett.* **141**, 1405–1419 (2011). doi:10.1007/s10562-011-0675-2

30. Y. Chauvin, A. Hirschauer, H. Olivier, Alkylation of isobutane with 2-butene using 1-butyl-3-methylimidazolium chloride—Aluminium chloride molten salts as catalysts. *J. Mol. Catal.* **92**, 155–165 (1994). doi:10.1016/0304-5102(94)00065-4

31. R. Kore, P. Berton, S. P. Kelley, P. Aduri, S. S. Katti, R. D. Rogers, Group IIIA halometallate ionic liquids: Speciation and applications in catalysis. *ACS Catal.* **7**, 7014–7028 (2017). doi:10.1021/acscatal.7b01793

32. H. K. Timken, H. Luo, B.-K. Chang, E. Carter, M. Cole, in *Commercial Applications of Ionic Liquids*, M. B. Shiflett, Ed. (Springer, 2020), pp. 33–47.

33. N. R. Jaegers, K. T. Mueller, Y. Wang, J. Z. Hu, Variable temperature and pressure operando MAS NMR for catalysis science and related materials. *Acc. Chem. Res.* **53**, 611–619 (2020). doi:10.1021/acs.accounts.9b00557 Medline

34. N. R. Jaegers, W. Hu, Y. Wang, J. Z. Hu, High-temperature and high-pressure in situ magic angle spinning nuclear magnetic resonance spectroscopy. *J. Vis. Exp.* **164**, e61794 (2020). Medline

35. Y. Zhang, R. Zhao, M. Sanchez-Sanchez, G. L. Haller, J. Hu, R. Bermejo-Deval, Y. Liu, J. A. Lercher, Promotion of protolytic pentane conversion on H-MFI zeolite by proximity of extra-framework aluminum oxide and Brønsted acid sites. *J. Catal.* **370**, 424–433 (2019). doi:10.1016/j.jcat.2019.01.006

36. J. Weitkamp, Catalytic hydrocracking—Mechanisms and versatility of the process. *ChemCatChem* **4**, 292–306 (2012). doi:10.1002/cctc.201100315

37. M. Shi, J. Jiang, H. Zhao, Electrodeposition of aluminum in the 1-ethyl-3-methylimidazolium tetrachloroaluminate ionic liquid. *Electrochem* **2**, 185–196 (2021). doi:10.3390/electrochem2020013

38. T. Welton, Room-temperature ionic liquids. Solvents for synthesis and catalysis. *Chem. Rev.* **99**, 2071–2084 (1999). doi:10.1021/cr980032t Medline

39. J. Estager, A. A. Oliferenko, K. R. Seddon, M. Swadźba-Kwaśny, Chlorometallate(III) ionic liquids as Lewis acidic catalysts—A quantitative study of acceptor properties. *Dalton Trans.* **39**, 11375–11382 (2010). doi:10.1039/c0dt00895h Medline

40. J. Z. Hu, M. Y. Hu, Z. Zhao, S. Xu, A. Vjunov, H. Shi, D. M. Camaioni, C. H. F. Peden, J. A. Lercher, Sealed rotors for in situ high temperature high pressure MAS NMR. *Chem. Commun.* **51**, 13458–13461 (2015). doi:10.1039/C5CC03910J Medline

41. R. Kore, S. P. Kelley, A. D. Sawant, M. K. Mishra, R. D. Rogers, Are ionic liquids and liquid coordination complexes really different? - Synthesis, characterization, and catalytic activity of $AlCl_3$/base catalysts. *Chem. Commun.* **56**, 5362–5365 (2020). doi:10.1039/D0CC01452D Medline

42. R. Kore, S. P. Kelley, P. Aduri, R. D. Rogers, Mixed metal double salt ionic liquids comprised of $[HN_{222}]_2[ZnCl_4]$ and $AlCl_3$ provide tunable Lewis acid catalysts related to the ionic environment. *Dalton Trans.* **47**, 7795–7803 (2018). doi:10.1039/C8DT00976G Medline

43. X. Shen, T. Sun, L. Yang, A. Krasnoslobodtsev, R. Sabirianov, M. Sealy, W.-N. Mei, Z. Wu, L. Tan, Ultra-fast charging in aluminum-ion batteries: Electric double layers on active anode. *Nat. Commun.* **12**, 820 (2021). doi:10.1038/s41467-021-21108-4 Medline

44. P. Hu, R. Zhang, X. Meng, H. Liu, C. Xu, Z. Liu, Structural and spectroscopic characterizations of amide-$AlCl_3$-based ionic liquid analogues. *Inorg. Chem.* **55**, 2374–2380 (2016). doi:10.1021/acs.inorgchem.5b02744 Medline

45. F. Coleman, G. Srinivasan, M. Swadźba-Kwaśny, Liquid coordination complexes formed by the heterolytic cleavage of metal halides. *Angew. Chem. Int. Ed.* **52**, 12582–12586 (2013). doi:10.1002/anie.201306267 Medline

46. B. Gilbert, H. Olivier-Bourbigou, F. Favre, Chloroaluminate ionic liquids: From their structural properties to their applications in process intensification. *Oil Gas Sci. Technol.* **62**, 745–759 (2007). doi:10.2516/ogst:2007068

47. M. Angell, G. Zhu, M.-C. Lin, Y. Rong, H. Dai, Ionic liquid analogs of $AlCl_3$ with urea derivatives as electrolytes for aluminum batteries. *Adv. Funct. Mater.* **30**, 1901928 (2020). doi:10.1002/adfm.201901928

48. L. C. Brown, J. M. Hogg, M. Swadźba-Kwaśny, Lewis acidic ionic liquids. *Top. Curr. Chem. (Cham)* **375**, 78 (2017). doi:10.1007/s41061-017-0166-z Medline

49. Y. Li, R. Zhang, X. Meng, P. Ouyang, H. Liu, C. Xu, Z. Liu, Characterization and hydrogenation removal of acid-soluble oil in ionic liquid catalysts for isobutane alkylation. *Ind. Eng. Chem. Res.* **60**, 13764–13773 (2021). doi:10.1021/acs.iecr.1c02376